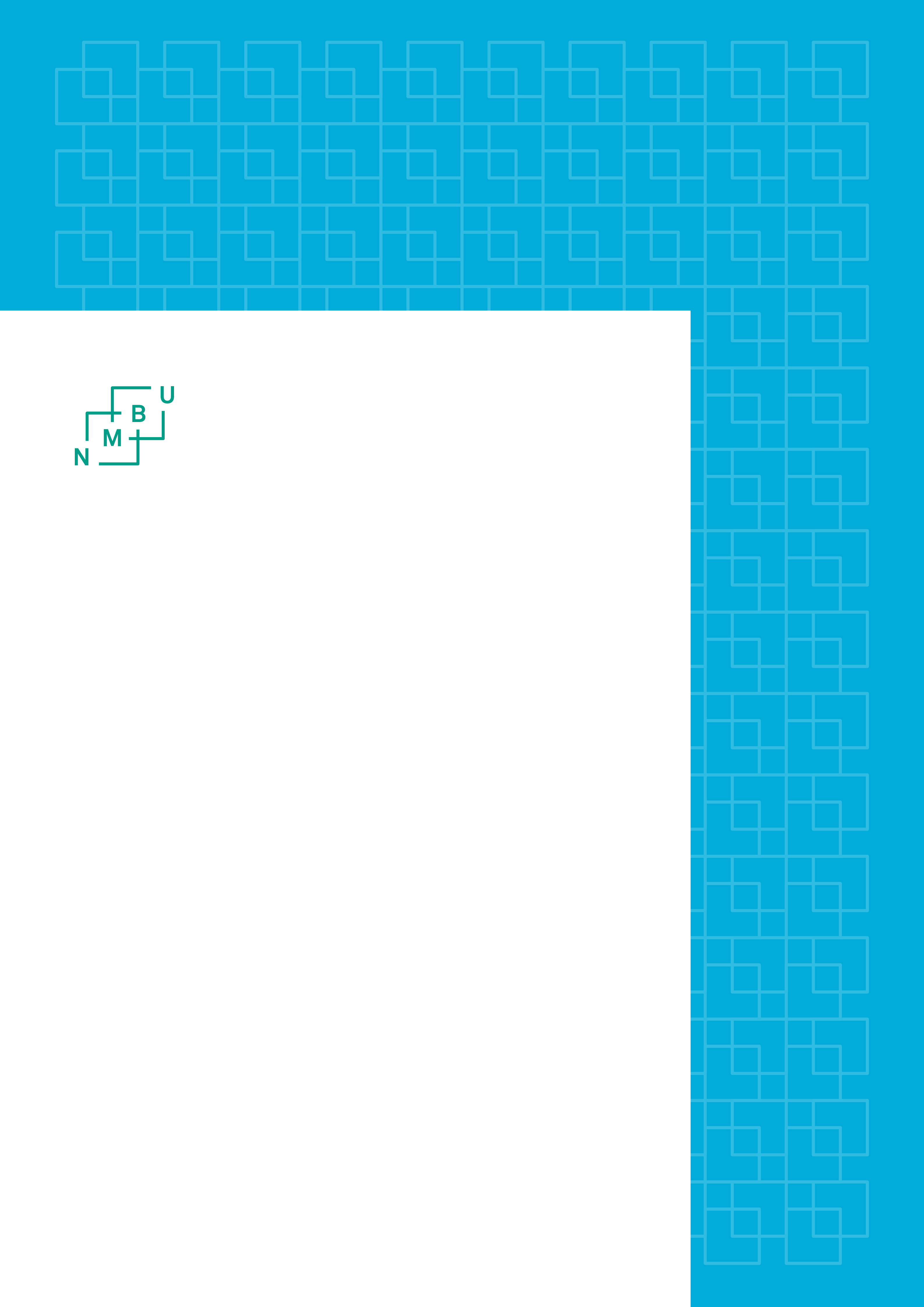
NMBU

NORWEGIAN UNIVERSITY OF LIFE SCIENCES

FACULTY OF ENVIRONMENTAL SCIENCE AND TECHNOLOGY

DEPARTMENT OF MATHEMATICAL SCIENCES AND TECHNOLOGY

Observations of Gravity Field Variations from Ground and Satellite Data

Author:
Alexander Helland

Supervisors:
Dr.-Ing. Christian Gerlach
Prof. Bjørn R. Pettersen

May 15, 2014

Abstract

The Earth's gravity field consists of several constituents of geophysical nature. By using geodetic observations techniques to observe gravity field variations, it is possible to monitor these geophysical processes.

This thesis tries to analyse how Earth's gravity field varies on a global and on a local scale. In addition, attempts have been made to offer geophysical explanations to the variations observed. Observational material gathered through terrestrial gravimetry from three different locations in Norway, as well as satellite data from GRACE, has been used to study Earth's gravity field.

Performing an analysis covering several years using terrestrial gravimetry data, shows how Norway is influenced by glacial isostatic adjustment (GIA). The GIA induced vertical displacement was estimated to be 8.7 mm for Ås and 8.0 mm for Trysil. The Trysil observations also reveal severe amounts of seasonal gravity variations, ranging from ± 4 microgals to ± 8 microgals. These seasonal gravity variations are correlated with the local hydrology cycle.

Using monthly GRACE solutions, this thesis shows how GIA influence Fennoscandia, northern parts of North America and Antarctica by increasing the regional mass distribution. Seasonal hydrology variations in the Amazon and southern parts of Africa can be detected by GRACE as well.

Finally, this thesis shows how GRACE and terrestrial data can detect some of the same gravity field variations. However, due to some methodology differences, the different gravity field signals behave differently.

Sammendrag

Jordens tyngdefelt består av flere geofysiske komponenter. Ved å ta i bruk geodetiske målemetoder, kan man observere og analysere disse geofysiske prosessene.

Denne oppgaven forsøker å analysere hvordan tyngdefeltet varierer globalt og lokalt. Gjennom analysen er det forsøkt å komme med geofysiske forklaringer til de ulike variasjonene som ble observert. Observasjonsmaterialet består av bakkebaserte tyngdedata, samlet fra tre ulike steder i Norge. Samtidig har observasjoner fra satelliten GRACE blitt tatt i bruk.

Analysen av bakkebaserte tyngdedata viser hvordan Norge påvirkes av landhevning etter forrige istid. Den vertikale forflytningen ble estimert til å være 8.7 mm i Ås og 8.0 mm i Trysil. Observasjonsmaterialet viser også at Trysil opplever store sesonvariasjoner. Disse variasjonene kan forklares av lokale hydrologiske variasjoner.

Ved å ta i bruk månedlige løsninger fra GRACE, har man observert at Fennoskandia, nordlige deler av Nord Amerika og Antarktisk påvirkes av landhevning i form av masseforflytning. GRACE kan også detektere sesongbaserte hydrologiske variasjoner i Amasonas og i de sørlige områdene av Afrika.

Til slutt i oppgaven har man forsøkt å se hvordan GRACE og bakkebasert gravimetri kan detektere noen av de samme geofysiske signalene tyngdefeltet består av.

Acknowledgement

This thesis summarizes my work during the last four months, as well as it marks the end of my student life at the Norwegian University of Life Sciences in Ås.

There are several people I wish to show my gratitude towards, who has helped me during the past four months. First of all, I would like to thank my supervisors Christian Gerlach and Bjørn Ragnvald Pettersen. They have offered explanations to all my questions, and guided me through this process. For this, I am very grateful!

A special thanks to Jon Glenn Gjevestad, who has thought me how to operate the FG5 instrument. In addition, he has spend many hours in the gravity lab these past four months, troubleshooting and maintaining the instrument.

Thanks to Vegard Ophaug! You have been my "turn-to-guy" when I needed someone to discuss my geodesy related problems.

Thanks to Kartverket and Ove Omang for letting me use their gravimetry data from Ny-Ålesund.

I would also like to thank my fellow students in room TF202 for general support and lots of laughter.

Finally I would like to thank my family and my dearest Åsa.

Alexander Helland

Ås, 2014/05/15

Contents

List of Figures

List of Tables

Chapter 1

Introduction

One of the most classical definitions of the word "Geodesy" was proposed by the German geodesist Friedrich Robert Helmert (1880). He quite accurately stated that *"geodesy is the science of the measurement and mapping of the Earth's surface"*. This definition holds true, even today. More recent and extended definitions of the word geodesy often include understanding Earth's orientation and gravity field, in addition to determination of the geometric shape. With this extended definition, geodesy is linked to fields like geo- and engineering sciences, navigation and geomatics (Torge and Müller, 2012). The part of geodesy related to the physical properties of Earth's gravity field is often referred to as "Physical Geodesy".

Gravity consists of two constituents; gravitational acceleration and centripetal acceleration. The gravitational force is directly linked to the mass of a body, and the centripetal force emerge due to a body's rotation around its own rotational axis. Gravity observations have been carried out at least since the 18th century, and a wide variety of methods have been used since then. Today, gravity observations are carried out using gravimeters placed e.g. on the ground, on boats or in aeroplanes. In addition, space based methods like SLR and dedicated gravity satellite missions like CHAMP, GRACE and GOCE are used to determine Earth's gravity field.

1.1 Motivation

The most common functional of Earth's gravity field is the geoid. The geoid is an equipotential surface and acts as a reference for determination of physical heights (e.g. orthometric heights). The geoid is often referred to as mean sea level, as it partly coincides with the surface of the oceans. A calculated mean geoid, however, does not coincide with the ocean surface. This deviation is known as sea surface topography, and is used in oceanography.

Many of the different components Earth's gravity field consists of is of geophysical nature. Especially the components that make Earth's gravity field exposed to temporal variations, which will be further discussed in chapter 2 of this thesis. Therefore, geodetic observation methods can be used to study these geophysical signals. The Gravity Recovery and Climate Experiment (GRACE) provides monthly gravity field solutions. In this way, short term gravity field variations can be derived. The spatial resolution of GRACE is somewhat limited, which means only global an regional short term variations can be estimated.

1.2 Thesis objective

This thesis will investigate how geodetic observation techniques can detect gravity field variations. These variations will further be discussed from a geophysical point of view. While doing so, this thesis will try to answer the following questions:

- How does the Earth's gravity field vary on a global scale?
- How does the Earth's gravity field vary on a local scale?
- What causes these gravity field variations?
- Can satellite observations and terrestrial observations detect some of the same gravity field variations?

In order to detect gravity field variations, a time variable obviously needs to be included. For that reason, satellite based and terrestrial observations mainly gathered between 2003 and present day are used to answer these questions.

1.3 Thesis summary

This thesis contains seven chapters. The content in each chapter is, in short, given in the following list.

- **Chapter 1: Introduction**
  This chapter gives an introduction to some geodetic definitions and physical geodesy. Furthermore, the thesis motivation and objective get discussed.

- **Chapter 2: The gravity field of the Earth**
  This chapter contains the theory related to Earth's gravity field and potential theory. It describes how gravity field determination can be carried out using spherical harmonic synthesis. And finally, an introduction to geophysical signals found in Earth's gravity field is given.

- **Chapter 3: Observational methods and technology**
  This chapter describes different ways of observing Earth's gravity field, both by using terrestrial and space based techniques.

- **Chapter 4: Local gravity variations from terrestrial data**
  This chapter contains the results when attempting to derive local gravity variations from terrestrial data. Observations from three different stations have been analysed.

- **Chapter 5: Global gravity field variations from GRACE**
  This chapter contains the results when attempting to derive global gravity variations from space based data. Used in this analysis is data gathered by the dedicated gravity satellite GRACE.

- **Chapter 6: Comparison of terrestrial and satellite based gravity variations**
  This chapter contains a comparison of terrestrial and space based data. The main goal was to see if the different techniques display some of the same temporal variations in Earth's gravity field.

- **Chapter 7: Conclusions and further outlook**
  This chapter finalises the thesis by drawing conclusions from the obtained results. Finally, a further outlook is given.

1.4 Abbreviations

This section provides some explanatory words on abbreviations used in this thesis.

GNSS	Global Navigation Satellite Systems
VLBI	Very Long Baseline Interferometry
SLR	Satellite Laser Ranging
SST	Satellite to Satellite Tracking
GRACE	Gravity Recovery and Climate Experiment
CHAMP	Challenging Mini-satellite Payload
GOCE	Gravity field and Steady-State Ocean Circulation Explorer
FG	Field Gravimeter
SCG	Superconducting gravimeter
NASA	National Aeronautics and Space Administration
ESA	European Space Agency
DLR	The German Aerospace Center
RDC	GRACE Raw Data Center
GFZ	GeoForschnungsZentrum
CSR	Center for Space Research (University of Texas)
JPL	Jet Propulsion Laboratory, NASA
IGG	Institute for Geodesy and Geoinformation, Bonn university
AIUB	Astronomical Institute University of Bern
ICGEM	International Centre for Global Earth Models
IERS	International Earth Rotation and Reference Systems Service
ECGS	European Center for Geodynamics and Seismology
NMBU	Norwegian University of Life Sciences
GIA	Glacial Isostatic Adjustment
APL	Atmospheric Pressure Loading
SWE	Snow Water Equivalent
EWH	Equivalent Water Height
SHS	Spherical Harmonic Synthesis
EOF	Empirical Orthogonal Function
PCA	Principal Component Analysis

Chapter 2

The gravity field of the Earth

Physical geodesy is the theory and studies related to Earth's gravity field. One of the main goals in physical geodesy is to determine Earth's gravity field globally from observations taken on or near the Earth's surface. Gravity field determination often involves solution of differential equations with certain boundary conditions. The well known Newton's law of universal gravitation (see equation 2.1) is hence not sufficient.

$$F = \frac{GMm}{r^2} \tag{2.1}$$

This chapter describes properties and observation quantities related to the Earth's gravity field, including temporal variations. In addition, a description of how to determine the Earth's gravity field using potential theory is given.

2.1 Properties and observation quantities

Newton's law of universal gravitation generates a gravitation point value for an item with mass m at a distance r from Earth's centre of mass, when the gravitational constant G and Earth's mass M are assumed known. The equation can be expanded to a vector field, as shown in equation 2.2.

$$\vec{F} = F(-\frac{\vec{r}}{r}) = -\frac{GMm}{r^3}\vec{r} \tag{2.2}$$

In equation 2.2, $\vec{r}$ is the unit vector in a three dimensional space. If no external forces, except the gravitational force, are acting on a body, the gravitation $\vec{g}$ can be expressed as

$$\vec{F} = m\vec{g} = -\frac{GMm}{r^3}\vec{r} \quad \Longrightarrow \quad \vec{g} = -\frac{GM}{r^3}\vec{r} \tag{2.3}$$

Potential theory states that if a vector field is conservative,[1] it has a corresponding potential function given as

$$\vec{g} = \nabla V = \frac{\delta V}{\delta x}\vec{i} + \frac{\delta V}{\delta y}\vec{j} + \frac{\delta V}{\delta z}\vec{k} \tag{2.4}$$

where V is the corresponding potential function to the gravitational field $\vec{g}$ (Hofmann-Wellenhof and Moritz, 2006). It can be proved that Earth's gravitational field is conservative by showing $curl(\vec{g}) = 0$. The gravitational potential is easier to handle, as it is a scalar field and not a vector field. From a mathematical point of view, the gravitational potential is given as

$$V = \frac{GM}{r} + C \tag{2.5}$$

where C is an arbitrary constant. Due to this constant, it is only possible to determine potential differences and not an absolute potential. However, C is often set to zero. Through the principle of superposition, the attraction from the Earth on a unit point mass can be expressed as

$$V = \sum_{Earth} \frac{GM_i}{r} \tag{2.6}$$

---

[1] Conservative vector fields have no change in the internal energy balance, as well as no field rotation.

where M_i is the mass of a small mass-unit inside Earth's surface (Hofmann-Wellenhof and Moritz, 2006). By inserting density instead of mass ($\rho = \frac{dM}{dv}$) the potential can be expressed on integral form.

$$V = G \iiint\limits_{Earth} \frac{1}{r} \rho dv \tag{2.7}$$

Equation 2.7 is known as Newton's integral. The density of the Earth is impossible to determine exact. Therefore, the integral is transferred to a differential equation, which is more suitable when dealing with boundary value problems. This way Poisson's equation emerges (equation 2.8).

$$\nabla^2 V = \frac{\delta^2 V}{\delta x^2} + \frac{\delta^2 V}{\delta y^2} + \frac{\delta^2 V}{\delta z^2} = -4\pi G \rho \tag{2.8}$$

Poisson's equation is basically an additional way, differing from Newton's law of universal gravitation, of representing Earth's attraction on a unit point mass. If the point mass is located outside Earth's surface the density is equal to zero, and Poisson's equation is reduced to Laplace' equation (equation 2.9).

$$\nabla^2 V = \frac{\delta^2 V}{\delta x^2} + \frac{\delta^2 V}{\delta y^2} + \frac{\delta^2 V}{\delta z^2} = 0 \tag{2.9}$$

Potential functions that satisfy Laplace' equation are called harmonic functions. It is easy to find a set of solutions that satisfy Laplace' equation. However, the problem gets more complex when strict boundary conditions are present, which is the case when attempting to describe the Earth's gravitational field. Because the Earth is rotating, we are forced to operate with gravity and gravity potential, rather than gravitation and gravitational potential. The gravitational potential V is given as

$$V = W - V_c \Longrightarrow \vec{g} = \nabla W \tag{2.10}$$

where W is the gravity potential and V_c is the rotational potential.[2] Like earlier

---

[2] The rotational potential is not harmonic, but can be estimated using: $V_c = \frac{1}{2}\omega_e^2(x^2 + y^2)$.

stated, it is only possible to determine potential differences. This is why some adjustments have to be made:

- Earth's ellipsoid is given a mass, which makes it an object with existing attractional force
- Earth's ellipsoid is given an angular velocity, allowing the object to rotate
- Positions on Earth's ellipsoid is expressed in spherical coordinates
- Earth's surface is replaced by the geoid[3]

The first two bullets above create a model, also known as a geodetic reference system. Two examples of geodetic reference systems are GRS80 and WGS84. The geoid is an equipotential surface, and therefore easier to handle. If we now introduce ellipsoidal potential (also known as normal potential) U, the potential difference can be expressed as a disturbing potential

$$T = (W - V_c) - (U - V_c) = W - U \tag{2.11}$$

where W is geoid potential. The disturbing potential can be calculated using, for instance, Stoke's integral (equation 2.12), Neumann-Koch's function (equation 2.13) or spherical harmonic synthesis (section 2.2).

$$T = \frac{R}{4\pi} \iint\limits_{\sigma} S(\psi) \Delta g d\sigma \tag{2.12}$$

$$T = \frac{R}{4\pi} \iint\limits_{\sigma} K(\psi) \delta g d\sigma \tag{2.13}$$

Stoke's integral use gravity anomalies Δg to calculate disturbing potential. Gravity anomalies are the gravity difference between geoid gravity and ellipsoid gravity, also known as normal gravity. Nowadays, GNSS provide highly accurate ellipsoidal heights, which make it possible to derive normal gravity at the geoid. This can be

---

[3] Except in the case of Molodensky, where Earth's surface is chosen as boundary instead of the geoid.

used to calculate gravity disturbance δg instead of gravity anomalies. The gravity disturbance is used in Neumann-Kock's function to calculate disturbing potential.

2.2 Spherical harmonic representation

In spherical harmonic representation, we add up all the solutions to Laplace' equation (equation 2.9), in a way that the sum will satisfy the boundary conditions (Hofmann-Wellenhof and Moritz, 2006). Doing this for spherical coordinates, the result is a spherical harmonic function given as

$$V(r,\theta,\lambda) = \frac{GM}{R}\sum_{n=0}^{\infty}\left(\frac{R}{r}\right)^{n+1}\sum_{m=0}^{n} P_{nm}(\cos\theta)[C_{nm}\cos(m\lambda)+S_{nm}\sin(m\lambda)] \quad (2.14)$$

where GM is the product of Newtons gravitational constant and the mass of the Earth and R is the mean Earth radius. $(R/r)^{n+1}$ is the "upward continuation factor", which lets us calculate the potential at an arbitrary geocentric distance r. This factor serves as a mitigation of the signal. P_{nm} is the so called Legendre functions that emerge when series expansion of $1/r$ is carried out. The Legendre functions have to be taken into account due to use of spherical coordinates. C_{nm} and S_{nm} are dimensionless potential coefficients, and finally n and m indicate degree and order. Calculating potential from amplitudes of the gravity field signal is known as spherical harmonic synthesis. If the corresponding coefficients from the normal potential U are subtracted from the potential coefficients, it is possible to express disturbing potential through the spherical harmonic representation as

$$T(r,\theta,\lambda) = \frac{GM}{R}\sum_{n=2}^{\infty}\left(\frac{R}{r}\right)^{n+1}\sum_{m=0}^{n} P_{nm}(\cos\theta)[\Delta C_{nm}\cos(m\lambda)+\Delta S_{nm}\sin(m\lambda)] \quad (2.15)$$

where

$$\Delta C_{nm} = \begin{cases} C_{nm} - U_{nm} & \text{if } m = 0 \text{ and } n \in \{2, 4, 6, 8, ..., N_{max}\} \\ C_{nm} & \text{else} \end{cases}$$

$$\Delta S_{nm} = S_{nm}$$

The reason for the different behaviour for odd- and even numbered degrees in the cosine coefficients above is due to symmetry about equator. The sine coefficients are the same after subtraction of normal potential coefficients, and this is due to symmetry about the rotational axis. The summation begins at spherical harmonic degree 2. The zero-degree term disappears as the mass and equatorial radius of the geodetic reference is most often equal to the mass an equatorial radius of the Earth. The first degree term disappears when the two centre of masses coincide (Gerlach, 2003).

A global potential model contains a set of potential coefficients, which can be used to calculate different gravity quantities such as disturbing potential T, geoid height N, gravity anomaly Δg and gravity disturbance δg. The only thing that separates these quantities in the spectral domain are different upward continuation factors and spectral eigenvalues (see table 2.1), which means it is easy to go from one quantity to another.

Table 2.1: Spherical harmonic synthesis of gravity field quantities

T	$=$	$\frac{GM}{R}$	$\sum_{n=2}^{\infty}$	$\left(\frac{R}{r}\right)^{n+1}$		$\sum_{m=0}^{n} P_{nm}[\Delta C_{nm}\cos(m\lambda) + S_{nm}\sin(m\lambda)]$
N	$=$	R	$\sum_{n=2}^{\infty}$	$\left(\frac{R}{r}\right)^{n+1}$		$\sum_{m=0}^{n} P_{nm}[\Delta C_{nm}\cos(m\lambda) + S_{nm}\sin(m\lambda)]$
Δg	$=$	$\frac{GM}{R^2}$	$\sum_{n=2}^{\infty}$	$\left(\frac{R}{r}\right)^{n+2}$	$(n-1)$	$\sum_{m=0}^{n} P_{nm}[\Delta C_{nm}\cos(m\lambda) + S_{nm}\sin(m\lambda)]$
δg	$=$	$\frac{GM}{R^2}$	$\sum_{n=2}^{\infty}$	$\left(\frac{R}{r}\right)^{n+2}$	$(n+1)$	$\sum_{m=0}^{n} P_{nm}[\Delta C_{nm}\cos(m\lambda) + S_{nm}\sin(m\lambda)]$
T_{rr}	$=$	$\frac{GM}{R^3}$	$\sum_{n=2}^{\infty}$	$\left(\frac{R}{r}\right)^{n+3}$	$(n+1)(n+2)$	$\sum_{m=0}^{n} P_{nm}[\Delta C_{nm}\cos(m\lambda) + S_{nm}\sin(m\lambda)]$

One fundamental problem in potential theory is how to describe the potential everywhere, when all that is given is a potential value on a boundary s. This is known as Dirichlet's problem, and can be solved by harmonic expansion of $V(r, \theta, \lambda)$. One solution is called Poisson's integral (equation 2.16), which is a significant formula in potential theory.

$$V_e(r, \theta, \lambda) = \sum_{n=0}^{\infty} \left(\frac{R}{r}\right)^{n+1} \frac{2n+1}{4\pi} \int\limits_{\lambda'=0}^{2\pi} \int\limits_{\theta'=0}^{\pi} V(r, \theta, \lambda) P_n(\cos\theta) \sin\theta' d\theta' d\lambda' \quad (2.16)$$

Spherical harmonic synthesis is one of the most commonly used methods when calculating gravity field quantities. "A pocket guide to physical geodesy" (see figure 2.1) explains how the potential signal behaves when applying different upward continuation factors and spectral eigenvalues. The upward continuation factor smooths the signal, and the spectral eigenvalues performs an anti-smoothing of the signal.

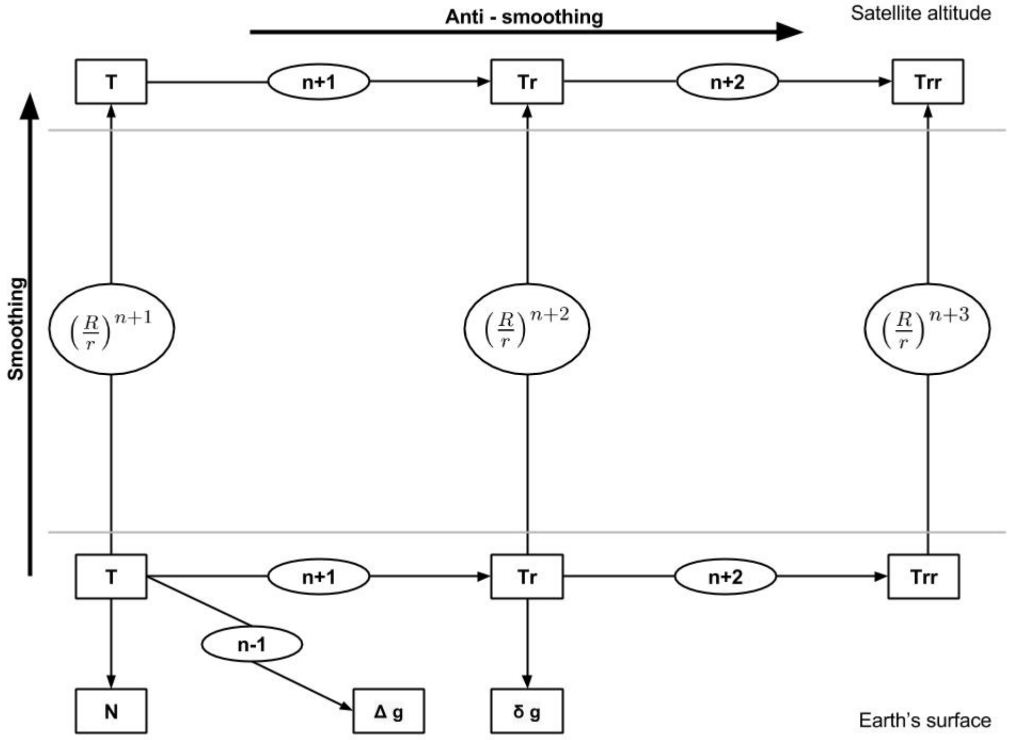

Figure 2.1: A pocket guide to physical geodesy.

2.2.1 Statistics related to spherical harmonic synthesis

In order to look at the content in a gravity field signal, the term degree variance has been introduced. Degree variances describe how much the signal varies at a certain spherical harmonic degree or in a certain spectral window. It can be used to analyse the signal content or signal strength. Degree variance differs from the more commonly used error variance, which is used to calculate, for instance, observation errors in statistical analysis. The dimensionless degree variances c_n can be expressed as

$$c_n = \sum_{m=0}^{n} [\Delta C_{nm}^2 + S_{nm}^2] \tag{2.17}$$

where ΔC_{nm} and S_{nm} are the spherical harmonic coefficients. By using spectral eigenvalues and scaling factors corresponding to gravity field quantities, it is now possible to calculate degree variances for geoid height, gravity anomaly, gravity disturbance etc.

$$c_n^N = R^2 \sum_{m=0}^{n} [\Delta C_{nm}^2 + S_{nm}^2] \tag{2.18}$$

$$c_n^{\Delta g} = \sum_{n=2}^{\infty} \left(\frac{GM}{R^2}(n-1) \right)^2 \sum_{m=0}^{n} [\Delta C_{nm}^2 + S_{nm}^2] \tag{2.19}$$

When people first started analysing and comparing signals from different potential models, it was observed that the degree variances were quite similar. Because most potential models describe the same gravity field,[4] the signal from different models does not vary much. Therefore, some theoretical degree variance models have been presented, as a rule of thumb. The two most frequently used are the degree variance models Kaula and Tscherning/Rapp, both named after the inventors. Kaula is based on potential coefficients, whereas Tscherning/Rapp is based on gravity anomalies. Kaula's degree variance model is given as

---

[4] There has been made some potential models for other planets, as well as for the moon.

$$c_n = 0.5\frac{1.6 \times 10^{-10}}{n^3} \qquad n > 0 \tag{2.20}$$

where n is spherical harmonic degree. By multiplying c_n with proper spectral eigenvalues and scaling factors, it can be used to describe degree variances for any given gravity field quantity. The Tscherning/Rapp model used to calculate degree variance for gravity anomalies can be written as

$$c_n^{\Delta g} = s^{n+2}\frac{A(n-1)}{(n-2)(n+B)} \qquad n \geq 3 \tag{2.21}$$

where A, B, s are all given constants and n is spherical harmonic degree. A is equal to 425.28 $mGal^2$, B is equal to 24 and s is equal to 0.999617. To avoid singularity n has to start at degree 3, and therefore the model has a given c_n at degree 2 equal to 7.5 $mGal^2$.

Since almost every potential model describes the same gravity field, and therefore has quite similar signals, it is often more interesting to compute error degree variances. Error degree variances are calculated using the coefficient errors included in the potential model, instead of the coefficients themselves. When degree variances and error degree variances are plotted in the same figure it is possible to determine an actual model resolution in terms of spherical harmonic degree. The actual model resolution is found where the degree variance- and the error degree variance curves intersect. This is where the signal to noise ratio is equal to one, and above this resolution the noise is greater in magnitude than the signal itself.

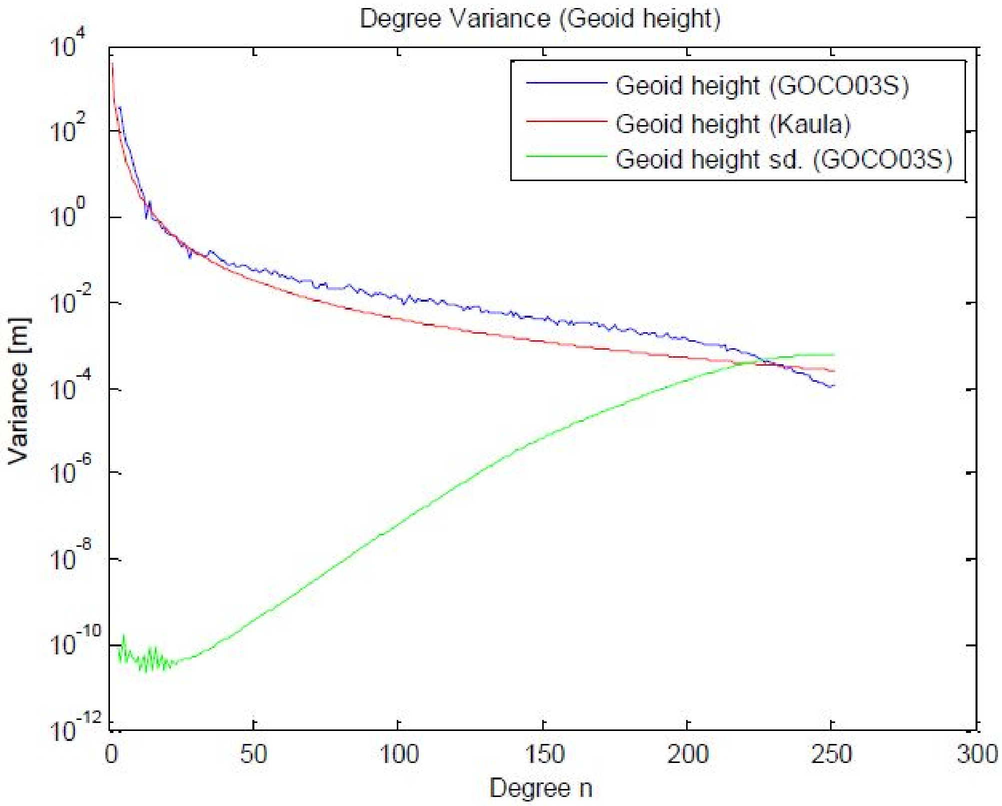

Figure 2.2: Degree variance and error degree variance computed from the GOCO03S potential model.

Figure 2.2 displays degree variance and error degree variance computed from the GOCO03S model. This model is complete to degree and order 250, but as shown in figure 2.2 the actual resolution is approximately 225. For all statical satellites only models (like GOCO03S), the actual resolution is lower than the model resolution. Also in this figure, the degree variance from the theoretical model Kaula is plotted. As shown, the two degree variance curves are quite similar.

The coefficient errors can also be used to calculate commission-error. This is an estimate of included errors in the potential models. However, Earth's potential contains information of higher order than any model can provide, and this is something that has to be taken into consideration. Omission-errors can be calculated using the theoretical models of e.g. Kaula or Tscherning/Rapp. By including higher degrees, it is possible to determine the magnitude of the errors that have been omitted. Adding the commission- and the omission-errors the model's total error is obtained.

2.3 Temporal gravity variations and geophysical signals

Earth's gravity field consists of several time varying geophysical signals, which make the gravity field exposed to temporal variations. These variations can be categorized as global effects, regional effects or local effects. Listed below are some of the most significant global effects.

- Earth rotation
- Polar motion

More regional effects are also very common. Some are more local than others, and have been specified in the list below.

- Solid Earth tides
- Ocean tides
- Ocean tide loading (Local)
- Atmospheric pressure loading (Local)
- Post glacial rebound
- Near-surface mass variation (Local)
  - Hydrology variations
  - Cryosphere variations

Some of the effects have a time variable of periodic nature, and others have time scales ranging from secular to episodic (Torge and Müller, 2012). This section tries to describe some of the main contributors to temporal gravity variations.

2.3.1 Variation in Earth's rotation

It has been established that gravity potential consists of two factors; gravitational- and rotational potential (see equation 2.10). This means that every change in Earth's rotation will directly influence Earth's gravity. The magnitude of the acceleration of gravity can be expressed as

$$g = |\nabla W| \tag{2.22}$$

where W is the gravity potential. In spherical coordinates (r, ϕ, λ) the acceleration of gravity can be expressed as

$$|\nabla W| = \sqrt{(V_r + \Phi_r)^2 + \left[\frac{1}{r\cos\phi}(V_\lambda + \Phi_\lambda)\right]^2 + \left[\frac{1}{r}(V_\phi + \Phi_\phi)\right]^2} \tag{2.23}$$

where V is gravitational potential and Φ is rotational potential, also known as centrifugal potential (Barthelmes, 2009). The lower indexes indicate partial derivatives with respect to each of the spherical coordinates. The rotational potential can be expressed as

$$\Phi = \frac{1}{2}\omega^2 r^2 (\cos\phi)^2 \tag{2.24}$$

where ω is the angular velocity of Earth's rotation. Any variation in this angular velocity will therefore propagate into Earth's gravity. The angular velocity of Earth's rotation, as well as the orientation of Earth's rotation axis, are subject to secular, periodic and irregular variations (Torge and Müller, 2012). These variations come from changes in external gravitational forces and internal geodynamical processes.

2.3.2 Polar motion

Earth's two poles are defined where the rotational axis intersects Earth's crust. A pole is thereby a point on the surface of the Earth, and this point's motion is called polar motion. The polar motion consists of two quasi-periodic oscillation components and one irregular drift parameter. One of the oscillation components is called "Chandler Wobble" and has a period of approximately 435 days (Torge and Müller, 2012). It is caused by mass variation on the surface of the Earth or internally. The other oscillation has an annual period, and is caused by seasonal mass variations. The polar drift is caused by motion in the Earth's core and mantle, as well as ice melting on large ice sheets (e.g. Greenland). The poles have drifted roughly 20 metres since 1900.

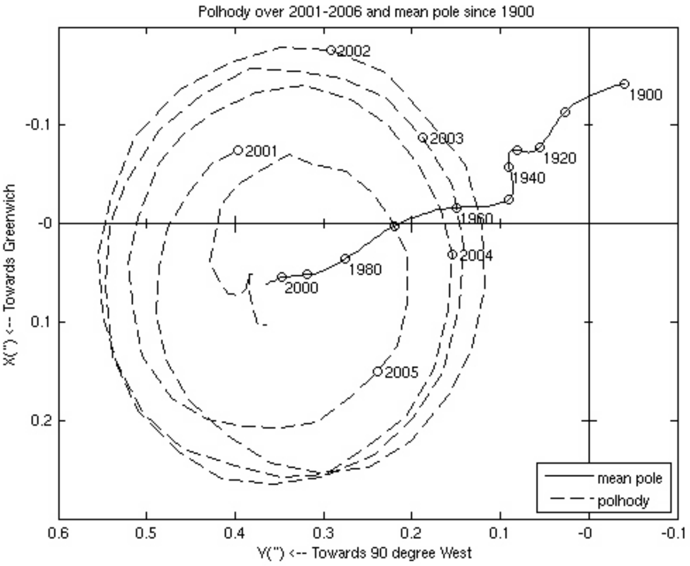

Figure 2.3: Polar oscillation since 2001 and polar drift since 1900. *Illustration: National Aeronautics and Space Administration (NASA)*

As shown in figure 2.3 the drift is irregular, and heading towards west. Due to two different oscillations the combined oscillation gets a pulsating effect (see figure 2.4). The combined period of the two oscillations is approximately 7 years.

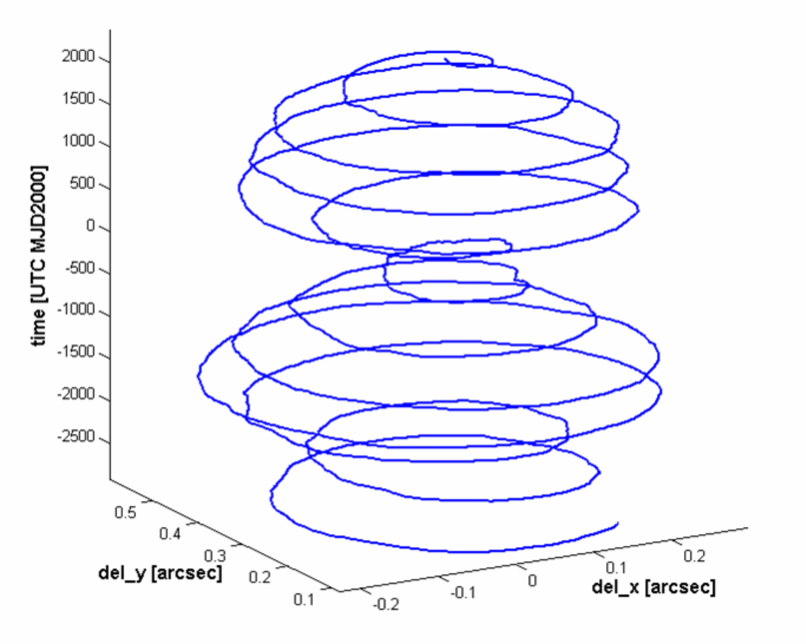

Figure 2.4: Polar oscillation. *Illustration: Wikipedia*

The deviation between current location of rotational axis and average location is given as

$$m_1 = x_p - \overline{x}_p \tag{2.25}$$

$$m_2 = -(y_p - \overline{y}_p) \tag{2.26}$$

Due to this deviation the rotational potential disturbance can be written as

$$\Delta\Phi(r, \theta, \lambda) = -\frac{\omega^2 r^2}{2} \sin 2\theta (m_1 \cos \lambda + m_2 \sin \lambda) \tag{2.27}$$

where ω is average angular velocity, r is geocentric distance and θ and λ are position-variables. Like stated above, the gravity potential consists of both gravitational potential and rotational potential, which means that polar motion has to be taken into account when attempting to determine the gravity potential. Polar motion models are made and distributed by the International Earth Rotation and Reference Systems Service (IERS).

2.3.3 Tidal and loading effects

Tidal effects on the Earth's body and the oceans are caused by lunisolar gravitation[5] and orbital accelerations (Torge and Müller, 2012). The orbital accelerations appear due to Earth's motion around the barycentre of a two-body system, like the Earth-Moon system and the Earth-Sun system. Solid Earth tides generate a mass variation locally, but more importantly, it raises every point on Earth which increases the geocentric distance from Earth's centre of mass.

Ocean tides generate a mass variation across the oceans and near coastal lines. Gravity is very dependent on mass, and local ocean tide variations therefore have to be taken into account. Due to mass variations generated by ocean tides, a secondary tidal effect emerge. This effect is called ocean loading. When ocean tides generates a mass displacement, Earth's crust will make a response. The response is in the form of deformations of the sea floor and a surface shift of nearby land (Sanz Subirana et al., 2011).

Atmospheric mass variations make the Earth's surface exposed to varying pressure. This geophysical phenomena is known as atmospheric pressure loading (APL). The variation in total atmospheric mass is almost entirely due to water vapour, which is caused by solar heating (Trenberth et al., 1987). The surface pressure oscillations have periods of diurnal and semi-diurnal solar days, and can cause vertical deformations of the Earth's crust ranging from 1 to 2 centimetres (Torge and Müller, 2012). APL effects have been observed in GNSS data, as well as in Very Long Baseline Interferometry (VLBI). These techniques are used to study geodynamics, which means that it is important to remove displacement signals caused by APL. The same goes for gravity satellites, like GRACE. In order to remove the APL signal, models have been generated. Modelling is based on global surface pressure data from weather forecasts (Boy and Hinderer, 2006).

---

[5] Other planets also play a part, but to a far lesser extent.

2.3.4 Post-glacial rebound

Post-glacial rebound, or Glacial Isostatic Adjustment (GIA), is the rise of landmasses that were depressed by huge ice sheets in the last glacial period (see figure 2.5). This period, more than 10000 years ago, led to a relative sea-level fall of about 120 meter. The corresponding amount of water was stored in massive ice sheets covering North America, Greenland, Scandinavia and Antarctica (GFZ, 2013). Due to load induced deformations during this period, these parts of the world experience GIA today.

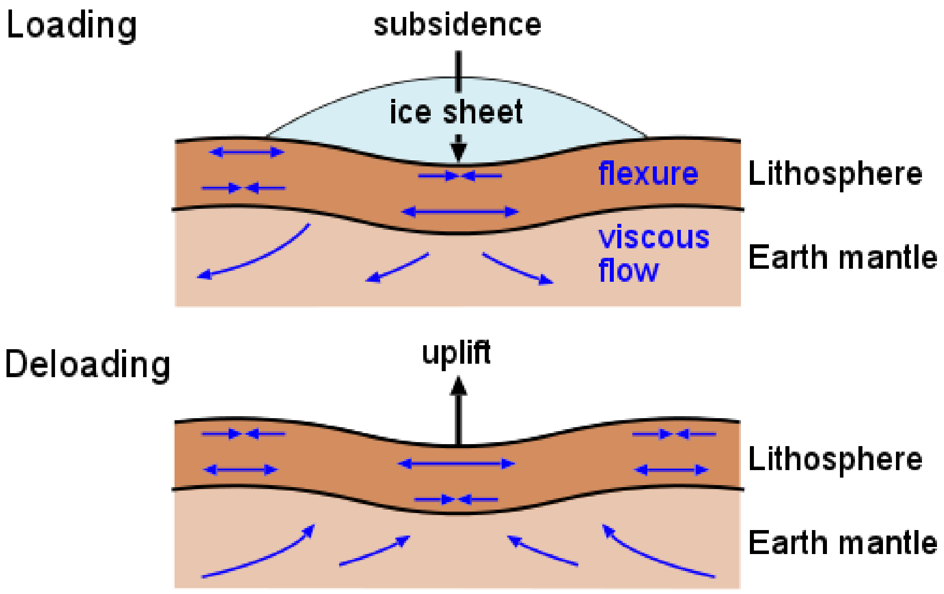

Figure 2.5: Glacial Isostatic Adjustment. *Illustration: GeoForschungsZentrum (GFZ)*

GIA influence the Earth's gravity field in the form of mass redistribution. Temporal variations occur as the masses within Earth's mantle are moving back towards where there previously was an ice sheet. Another gravity field related consequence due to GIA is increase in geocentric distance. With increased geocentric distance, the local gravity value will decrease by the amount corresponding to the gravity gradient at that point.

2.3.5 Near-surface mass variation

Near-surface mass variations also play a part in temporal gravity variations. These variations can mainly be categorized into hydrology variations and variations in the Earth's cryosphere. Hydrology is the study of water movement, distribution and quality. Almost 70 percent of the Earth's surface is covered by water in liquid state. Ocean currents are therefore a significant contributor to mass displacement on the Earth, which again lead to temporal gravity variations. Although most of Earth's water is found in the oceans, there is a large global distribution of groundwater. The amount of groundwater in the Earth's soil is very dependent on local meteorological aspects, such as rainfall and ice melting.

In addition to water in liquid state, the Earth has a great portion of frozen water as well. Almost two percent of Earth's entire water amount can be found in the cryosphere. The cryosphere include sea and lake ice, snow cover, glaciers, ice caps and frozen ground. When ice melts, large masses of water moves to different locations. This causes temporal gravity variations. With the average temperature of Earth's climate system rising, ice melting is something that will effect Earth's gravity field at a greater force in the future than we experience today.

In table 2.2, effects in terms of geoid height variation for some of the geophysical phenomena are listed.

Table 2.2: Temporal gravity variations (Peters, 2001)

Geophysical process	Spatial scale [km]	Period	Effect in terms of geoid heights [mm]
Solid-Earth and ocean tides	50 - 5000	Daily, semi-daily, semi-monthly	100 - 150
Atmosphere	20 - 2000	Yearly, seasonal, daily	15
Ocean currents	100 - 1000	Yearly, seasonal	10
Ocean surface	100 - 1000	Decades	1 - 3 per year
Continental water	10 - 8000	Yearly, seasonal	10 - 12
Cryosphere	100 - 1000	Seasonal, decades	1 - 3 per year
Earthquake	10 - 1000	Single event	0.5
Volcanic eruption	10 - 100	Single event	0.5
GIA	1000 - 10000	Secular	1 - 2 per year
Core an mantle	> 5000	Secular	0.005

Chapter 3

Observational methods and technology

Modelling of geodetic quantities, such as Earth's gravity field, is based on observations taken place on Earth's surface and in its exterior space (Torge and Müller, 2012). Although terrestrial observation techniques have been used to measure gravity since the 18th century, large areas of the Earth were not observed until the satellites made their entrance in the 20th century.[1] Today satellites provide global gravity field models, and by combining satellite- and terrestrial data the spatial- and spectral resolution of such models can be significantly improved.

This chapter will describe different techniques for measuring gravity, both terrestrial and space-based. The absolute gravity measurements carried out by the FG5 instrument and the GRACE satellite mission will receive most attention.

3.1 Terrestrial observations

Earth's gravity field has been observed for a long time, with the main goal to determine the shape of the Earth, also known as the geoid (Lysaker, 2011). In the 18th century pendulums were used to measure gravity. If a simplified pendulum example is used,[2] the period T is given as

---

[1] Sputnik 1 (launched 1957) was the first artificial satellite.

[2] Assuming the cord to be massless and a small maximum angular amplitude.

$$T \approx 2\pi\sqrt{\frac{L}{g}} \tag{3.1}$$

where L is the length of the cord holding a test mass and g is the local gravity value. If we solve for g and measure the period T, the local gravity value can be obtained. Note that the period is independent of mass, which holds true even for a real pendulum example.

Another technique used to measure gravity is free fall in vacuum. This method combines Newton's second law of motion and the equation of motion for uniform acceleration ($m\ddot{z} = mg(z)$), and the result is shown in equation 3.2.

$$z = z_0 + v_0 t + \frac{g}{2}t^2 \tag{3.2}$$

By measuring the drop-time t of a test mass in free fall between two known positions z and z_0, a local gravity value can be obtained. If the test mass is being dropped from rest, the initial velocity v_0 is zero.

The two methods described above both generate an absolute gravity value. There are also two relative methods that are used to calculate gravity differences. The first one is the spring method, where a test mass is connected to an elastic spring. The spring acts as a counterforce to the gravitational force and keeps the test mass in equilibrium position (Timmen, 2010). Hooke's law (equation 3.3) is then used to calculate the gravity difference Δg, when the change in spring length Δl is measured.

$$mg = k(l - l_0) \tag{3.3}$$

$$\Delta g = \frac{k}{m}\Delta l \tag{3.4}$$

In the equations above k is the spring constant and m is the mass of the test mass. The whole method is equivalent to a weight scale exposed to constant mass being transported between different positions. The difference in weight is explained by the gravity difference.

The final relative method, superconducting gravimetry, is perhaps the most complex one. The spring is in this case replaced by a magnetic suspension holding the test mass, and the test mass has the form of a hollow sphere (Neumeyer, 2010). The magnetic field has to be stable, and is created by currents in superconducting coils (Virtanen, 2006). A change in the Earth's mass will influence the test mass, and by monitoring the magnitude of this influence, gravity differences can be derived.

3.1.1 Instrumental overview

The methods described above are realized through different absolute and relative gravimeters (except the pendulum method which is outdated). In general the relative and the absolute gravimeters are complementing one another. The absolute gravimeter is depending on a relative gravimeter to provide a gradient, and the relative gravimeter (often) needs to be referred to an absolute gravity value.

The spatial resolution of terrestrial instruments is high compared to, for instance, satellite gravimetry. In gravity field modelling, terrestrial instruments account for the high frequencies and satellites account for the low frequencies.[3] The spatial resolution Δ is given as

$$\Delta = \frac{\pi R}{n} \approx \frac{20000km}{n} \tag{3.5}$$

where R is Earth's radius and n is spherical harmonic degree.

Spring-based relative gravimeters

Spring-based relative gravimeters (see figure 3.1) are the most common instrument when observing gravity. It can be used to calculate gravity differences between stations or temporal gravity variations at a specific point if the instrument is kept stationary over time. The expected accuracy for spring-based relative gravimeters is in the order of one to a few tens of microgals (Timmen, 2010).

---

[3] High frequencies means in this case more details locally.

Figure 3.1: LaCoste and Romberg relative gravimeter.

The method was first introduced in the 1930s. Relative gravimeters, like the one shown in figure 3.1, have a test mass that diverges from equilibrium position as a response to gravity differences. In order to restore the equilibrium position a dial has to be turned. This process is called ”nulling the beam” (Timmen, 2010). The number of turns is registered by a counter system and corresponds to a gravity difference. Counter units are transferred to units of gravity by proper scaling factors.[4] Nowadays, electronic feedback systems have replaced the mechanical system when restoring the equilibrium position. With an electronic feedback system the user will read the gravity differences expressed in milligal directly.[5] The observation equation used when dealing with a spring-based relative gravimeter (like LaCoste and Romberg) can be written as

$$g = N_0 + \sum_{j=1}^{p} d_j (t - t_0)^j + \sum_{k=1}^{m} Y_k z^k + \sum_{l=1}^{n} A_l \cos(\omega_l z - \phi_l) \tag{3.6}$$

where N_0 is a offset between instrumental level and absolute gravity datum, d_j is the drift parameter, Y_k is a calibration coefficient and z is the instrument reading. Last in the equation we have a periodic term where A is amplitude, ω_l is frequency and ϕ_l is the phase. The indexes j, k and l all indicated order of corresponding polynomial.

As we can see in equation 3.6, we have four different terms. The gravity datum is a choice that has to be made if the relative gravity value obtained from the instrument should be expressed as an absolute value. An instrumental drift is implemented in the second term, as the instrumental reading is vulnerable for environmental- or mechanical disturbances due to transportation. The instrumen-

---

[4] The gravity unit most frequently used is Gal ($Gal = cm/s^2$).

[5] However, the feedback needs to be scaled properly internally.

tal drift varies over time and therefore has to be estimated along with the gravity value. Often we assume this drift to be linear for small periods of time, although this does not always have to be the case. In order to determine the drift parameter, several methods for revisiting network points have been developed. Whether it is the profile-, star- or step method, they all strive to measure the same points several times, so that the drift parameter can be estimated. The third term is a calibration term, used to transform counter units into milligal. This term is reduced to just z if a gravimeter with an electronic feedback system is used. The fourth and final term is a periodic term which accounts for the periodic errors, due to mechanical errors in the instrument screws. This term is completely removed when using an electronic feedback system, as the screws are no longer needed to make observations. This, however, holds true only if the feedback system has a large enough range, which may cover 50 milligals. This is the case of the LaCoste and Romberg instrument.

Compared to other gravimeters the spring-based relative gravimeter is very portable, and therefore commonly used in field work. Since it only observes gravity differences it is depending on being referred to a gravity datum (see equation 3.6), although in some cases only gravity differences are of interest. Relative gravimeters have several geodetic applications:

- Providing additional gravity point values to improve regional geoids
- Provide a more dense gravity reference network
- Monitoring of temporal gravity changes
- Gradient determination

In order to obtain the expected accuracy some reductions have to be applied. Like the oceans, Earth's surface has a vertical motion due to lunar and solar attraction (see section 2.3.3). The magnitude of this motion varies as a function of position, and is of the order ± 20 - 30 centimetres which corresponds to approximately ± 150 microgals. If the Earth tide is not taken into account the gravity value obtained will be highly correlated with the tidal effects. A second reduction that needs to be taken into account is the instrumental height, i.e. height above the ground marker.

Superconducting relative gravimeters

The superconducting gravimeter (see figure 3.2) is a laboratory instrument, and was developed at the Univeristy of California in the late 1960s (Shiomi, 2009). It has a relative accuracy of 1 nanogal, making it the most precise instrument available today.

Figure 3.2: Superconducting gravimeter. *Photo: European center for geodynamics and seismology (ECGS)*

Instead of having an elastic spring to act as a counterforce on a test mass, the superconducting gravimeter has a magnetic field to keep the test mass in equilibrium position. Any deviation from equilibrium position is measured, and used to derive temporal gravity differences. The instrumental drift is usually very small and stable, i.e. linear even over several months.

Unlike the spring-based relative gravimeters, the superconducting gravimeter is not very portable. However, the instrument has several applications, and some of them are listed below:

- Highly precise gravity variations at a specific location
- Monitoring geophysical phenomena
- Testing gravitational physics

Due to instrument accuracy, observations carried out by both the superconducting- and the free fall absolute gravimeter have to be reduced. These reductions include Earth tide, polar motion, air pressure, instrumental reference height and ocean tide loading. Table 3.1 shows a list of influential elements, and how significant they are to gravity.

Table 3.1: List of contributors to Earth's gravity value

Magnitude $[ms^{-2}]$	Influential elements
10	Earth's gravitation
10^-2	Earth's flattening and rotation
10^-3	Mountains
10^-4	Inner mass distribution
10^-5	Large water reservoirs
10^-6	Solar/lunar tidal acceleration and distant earthquakes
10^-7	Changes in the cryosphere, hydrological changes and ocean tide loading
10^-8	Large buildings, post-glacial rebound, polar motion, changes in Earth's centripetal acceleration and atmospheric loading

Free fall absolute gravimeters

Like the superconducting gravimeter, the free fall absolute gravimeters are also laboratory instruments,[6] although not as stationary as the superconducting gravimeter. Due to their sensitivity and expected accuracy of 1-2 microgal, the instruments need to be operated in a stable environment. The free fall method was developed in the 1950s. However, the first transportable instrument was introduced in 1968 by *Faller* (Torge and Müller, 2012). An interferometer counts the number of maximums as a laser beam tracks a falling test mass in vacuum. The observations make several time-distance pairs, which then are used to calculate an absolute gravity value.

The most common instrument series within absolute gravimetry are the FG- and the A-series. The FG5 is the most accurate instrument available, but is also the least portable. The FG-L and A-10 instruments are made to be easier to use in fieldwork. They both have an expected accuracy of 10 microgals, whereas the

---

[6] Except the A-10 instrument, which can be operated outside.

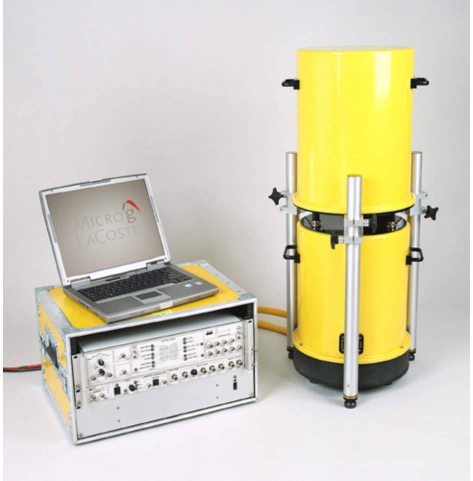

Figure 3.3: A10 absolute gravimeter. *Photo: Micro-g LaCoste Inc.*

FG5 has an expected accuracy of 1-2 microgals. Free fall absolute gravimeters are the only instruments which provide highly accurate absolute acceleration of gravity. This makes the instrument very important when creating a gravity reference network. Other applications are calibration of relative gravimeters and analysing geophysical phenomena. The observation equations used in absolute gravimetry are based on multiple time-distance measurement pairs in a least-square adjustment (Timmen, 2010). As the test mass falls through the dropping chamber, the gravity will change. The length of a typical dropping chamber is 20 centimetres, which means the acceleration of gravity will change approximately 60 microgals during the drop.[7] With an instrument accuracy of 1-2 microgals, it is obvious that a gradient needs to be included. Along with a gravity gradient, the initial position and velocity has to be taken into account. This means equation 3.2 has to be expanded to a power series, and the final observation equation is given as

$$z(t) = z_0(1 + \frac{1}{2}\gamma t^2 + \frac{1}{24}\gamma t^4) + v_0(t + \frac{1}{6}\gamma t^3) + \frac{1}{2}g_0(t^2 + \frac{1}{12}\gamma t^4) \tag{3.7}$$

---

[7] This is calculated using a standard gravity gradient of 3.08 $\mu Gal/\text{cm}$.

where z is current position, z_0 is initial position, v_0 is initial velocity, γ is the gravity gradient and t is time. Finally, g_0 is the derived free fall acceleration. The finite velocity of light, often known as c, must be taken into account when inserting time t into the observation equation.

$$t = t' + \frac{z}{c} \tag{3.8}$$

After this adjustment the least-square calculations can be carried out.

3.1.2 The FG5 absolute gravimeter

The FG5 instrument is the most accurate absolute gravimeter commercially available today. It mainly consists of a upper and lower chamber, an interferometer, an atomic clock and a laser (see figure 3.4). The vacuumized upper chamber, also known as the dropping chamber, contains a free falling corner cube. The cube is being transported to its starting position by a motorized drag-free cart. An ion pump is connected to the dropping chamber in order to maintain vacuum. This is necessary as the chamber is leaking. If the chamber withholds to many particles a vacuum pump has to be used in order to restore vacuum. The lower chamber, also known as the superspring chamber, contains a main spring and an internal reference corner cube. The main spring has a very large spring constant and serves as a stabilizer to the reference cube, allowing the cube not to be influenced by ground vibrations. The instrument also consists of a upper and lower tripod. The lower tripod supports the superspring chamber and the interferometer. The upper tripod supports the dropping chamber, physically separating the two parts.

The basic principle of the FG5 instrument is a laser beam entering the interferometer is separated by a beam splitter. One half goes directly into the light detector. The other half goes up and tracks the free falling cube on its way down, then goes all the way down and gets reflected by the reference cube. When the second beam gets back to the interferometer, it is recombined with the first beam and patterns of interference emerge. These patterns are also known as fringe patterns. By time-tagging the zero crossing of the interferometer fringe with a highly accurate atomic clock, the time-distance pairs are obtained.

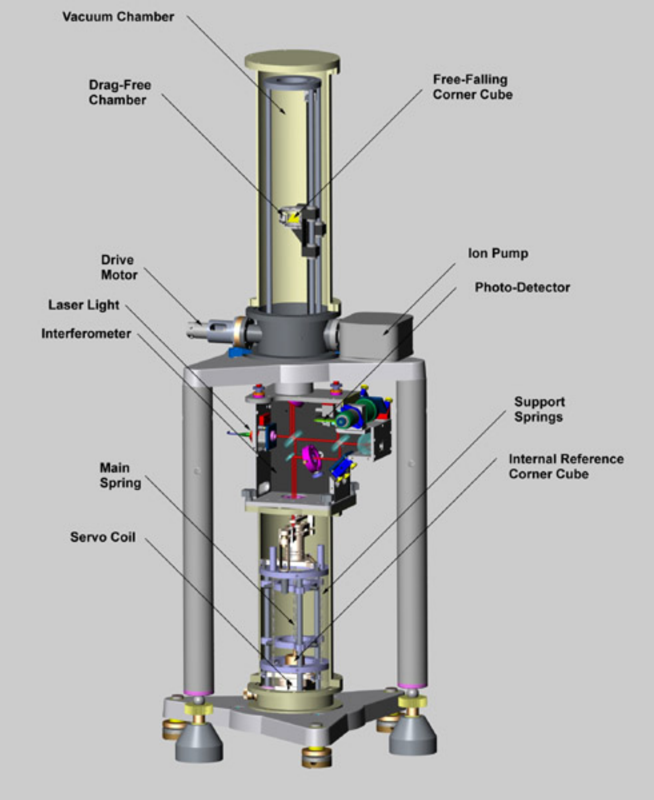

Figure 3.4: Schematic illustration of a FG5 absolute gravimeter. *Illustration: Micro-g LaCoste Inc.*

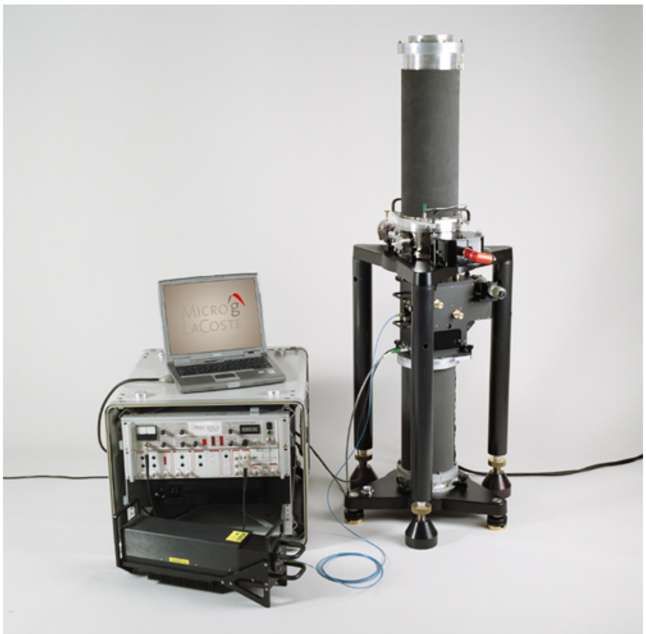

Figure 3.5: FG5 absolute gravimeter. *Photo: Micro-g LaCoste Inc.*

In order to generate a good gravity value, both the superspring chamber and the dropping chamber must be levelled. Also the beam has to be completely vertical, otherwise the gravity value obtained will only be a component of the absolute gravity value. A software is needed to add the necessary reductions to the observations (see table 3.1). A gravity point is normally determined on the ground, or at a given height above the ground, like 1.20 meters (which is the case for FG5 instruments). This means that a gradient also has to be typed into the software in order to reduce the measured gravity value to the reference position. The FG5 instruments often observe 24 sets distributed homogeneously over 24 hours. Every set consists of 50 drops, and the average over all drops is used as the final gravity value.

3.2 Satellite gravimetry

When satellites made their entrance in the mid 20th century, it became possible to model Earth's gravity field on a global scale. Using geodetic observation techniques such as Doppler, Satellite Laser Ranging (SLR) and satellite altimetry, gravity field models had a spatial resolution of about 500 km (half the wavelength) (Seeber, 2003). This corresponds to a spherical harmonic degree of approximately 36, and a geoid accuracy of 1 meter (see table 3.2). Today's requirements are about two orders of magnitude higher, which is achieved through dedicated gravity satellites such as CHAMP, GRACE and GOCE. These three missions have improved the spatial resolution and expected accuracy of global gravity field models significantly.

Table 3.2: Subdivision of the gravity field expansion (Seeber, 2003)

Subdivision	Long	Mean	Short	Very short
Wavelength [km]	> 8000	> 1000	> 200	< 200
SH degree [N]	< 5	< 36	< 200	> 200

Satellites are orbiting the Earth in a free-fall state, which means gravitation is observed and not gravity. In order to observe gravitational potential from satellites with the best accuracy possible, four requirements have been presented (Rummel et al., 2002). All these requirements have been considered in the realization of the satellite missions CHAMP, GRACE and GOCE:

1. The satellites have to be tracked continuously in three dimensions
2. Non-gravitational signals have to be measured and separated from the gravitational signals
3. The satellite orbits have to be as low as possible and near-polar
4. The measuring technique must counteract as the gravity field weakens with increasing altitude

The best global gravity field models today use data mostly acquired from SLR, CHAMP, GRACE and GOCE, as well as combining these observations with terrestrial observations. The following sections include a more detailed description of the space techniques SLR, CHAMP, GOCE and GRACE.

3.2.1 Satellite Laser Ranging (SLR)

Only few years into the satellite era work started on ways to track the satellites orbiting the Earth. At that time, space-based navigation systems like GPS were far off into the future, which meant that ground-based tracking techniques had to be developed. In 1961/62 development started in USA on pulsed laser-systems for tracking satellites (Seeber, 2003). This was realized when BEACON EXPLORER-B was launched in 1964, being the first satellite to carry laser-reflectors. The first successfully returned signal was obtained in 1965, and had an accuracy of a few meters (Vonbun et al., 1977). The range accuracy has improved since 1965, and today it is possible to measure the range to satellites with a precision of less than 1 cm (BKG, 2010).

The basic principle of SLR is to measure the travel time of a laser pulse when travelling up to a satellite and back down to the ground (see figure 3.6). In order to obtain an accurate range, a highly accurate atomic clock is needed. This way, every laser pulse that leaves the transmitter has a very accurate time tag, and the time difference measured is within today's accuracy requirement. The basic observation equation is very simple and can be written as

$$d = \frac{\Delta t}{2} c \tag{3.9}$$

where d is the distance between observatory and satellite, Δt is measured time difference of outgoing and returned laser pulse and c is the speed of light. The measured time difference has to be divided by a factor of two, as the laser pulse travels two times the distance between observatory and satellite.

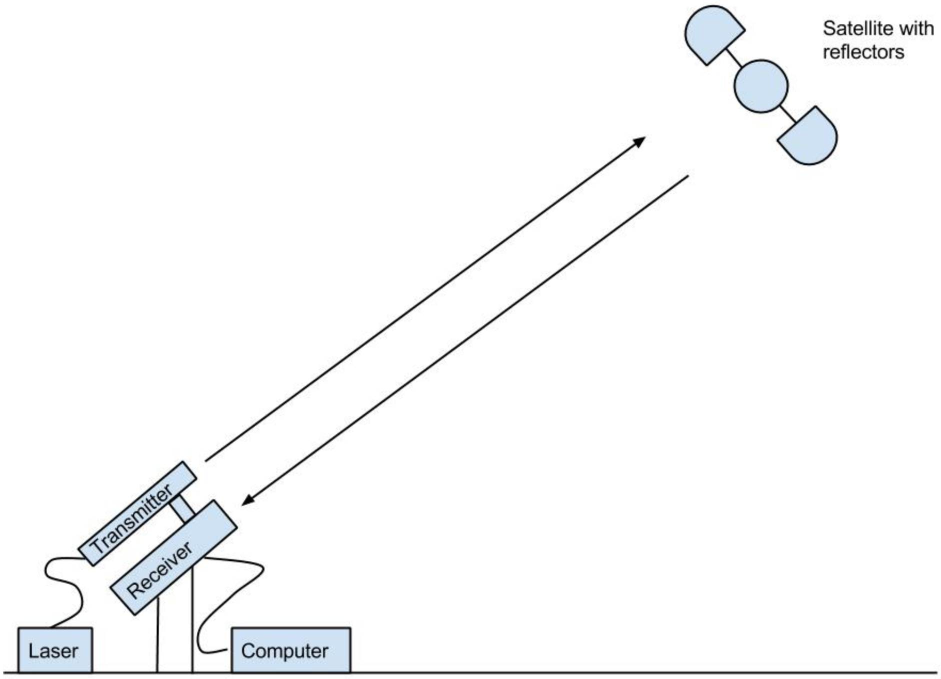

Figure 3.6: Basic principle of SLR.

Due to its accuracy potential, SLR has many applications in geodesy. These include:

- Contribution to reference frame establishment
  - Determination of geocentric coordinates
  - Determination of Earth orientation parameters like polar motion and variations in Earth's rotation
- Observing geodynamics
  - Measuring plate tectonics and crustal deformation
- Calculating precise satellite orbits
- Modelling Earth's gravity field
  - Observing gravitational orbit perturbation
  - Determination of the geocentric gravitational constant (GM)

Laser ranging has been used to compute Earth models since it became available in the late 1960s. The long time series with observations make SLR an important contributor to Earth modelling, even today. Satellite tracking can be used to analyse Earth's gravity field by observing gravitational orbit perturbations. SLR has a limited model resolution, as it only accounts for lower order coefficients. Also, the resolution is inversely proportional with orbit height (Seeber, 2003). This means that when the satellite orbit increases, the high frequent terms of the gravity field are damped. In 1995 a low altitude[8] German satellite, called GFZ-1, was launched with the main goal to improve the knowledge of the Earth's gravity field. With an orbital altitude of below 400 kilometres it was used to generate a satellite-only model called GRIM4-S4G, which was completed to a spherical harmonic degree of up to 100 (König et al., 1999).

Several models use SLR data today as well, particularly for the long-wavelength part of Earth's gravitational field. It is likely that SLR will continue to play a substantial part in gravity field modelling also in the future.

---

[8] Low Earth Orbit (LEO) means geocentric orbits ranging in altitude from 0 - 2000 km

3.2.2 The CHAMP satellite mission

The Challenging Mini-Satellite Payload for Geophysical Research and Application (CHAMP) was launched in July 2000, being the first dedicated gravity satellite in space. The main scientific goals of the mission were mapping of the global gravity- and magnetic field and profiling of the ionosphere and troposphere (Seeber, 2003). CHAMP realized one of two possible concepts within Satellite-to-Satellite Tracking (SST), known as the High-Low mode. The other concept (Low-Low mode) will be further explained in the GRACE section. In SST High-Low mode Global Navigation Satellite Systems (GNSS) are used to measure range changes between high orbiting navigation satellites and a low orbiting satellite, like CHAMP. In addition the satellite also carries laser reflectors, which means ground-based tracking (SLR) is available as well. However, SLR is only used for validation purposes in CHAMP's case.

Figure 3.7: CHAMP orbiting the Earth. *Illustration: GeoForschnungZentrum (GFZ)*

CHAMP was launched into a near-polar orbit (inclination of 87.3 degrees) and had an orbital altitude of 450 kilometres. Due to atmospheric drag, the altitude was expected to decrease to about 300 kilometres (Seeber, 2003). This decrease in altitude was intended by the developers to achieve a wider variety of coefficients. The initial mission duration was five years, but CHAMP continued to deliver data until it re-entered the Earth's atmosphere in September 2010. The basic principle of CHAMP was to have GPS satellites track its motion, in order to derive orbit perturbations. Star trackers were implemented to obtain the satellite's orientation. Gravity field modelling requires gravitational perturbations alone, which meant that other perturbations from disturbing elements like drag, solar radiation pressure and albedo had to be measured and separated from the gravitational perturbations. In CHAMP's centre of mass there was a three-axis accelerometer to measure all these non-gravitational accelerations acting on the spacecraft (Seeber, 2003). In this way the gravitational perturbations could be obtained and used to derive gravity field models.

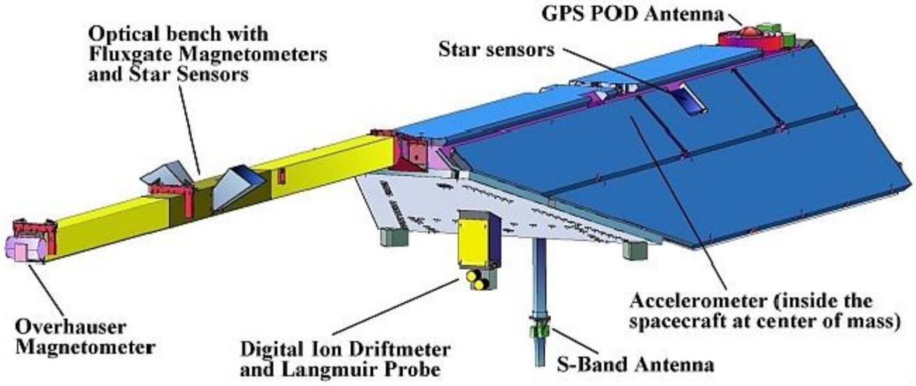

Figure 3.8: Schematic illustration of CHAMP. *Illustration: GeoForschnungZentrum (GFZ)*

CHAMP generated highly precise gravitational measurements. It significantly improved the accuracy and spatial resolution of global gravity field models, and will continue to be used in models for a long time into the future. Prior to CHAMP, the best gravity field model available was GRIM5-S1 (Biancale et al., 2000). It had a spatial resolution of 1500 kilometres and a geoid accuracy of 10 centimetres. If CHAMP data are used alone, it is possible to achieve a model with 400 kilometres spatial resolution and an accuracy of 5 centimetres, in terms of geoid determination (Reigber et al., 2005).

3.2.3 The GOCE satellite mission

The Gravity Field and Steady-State Ocean Circulation Explorer (GOCE) satellite mission was launched in March 2009, and used the same tracking system as CHAMP (SST, High-Low mode). It had an inclination of 96.5 degrees, and reached its observation altitude of 255 kilometres in September 2009 (Lysaker, 2011). Due to its very low orbit the planned mission duration was 20 months. However, the satellite continued to deliver data until October 2013, having orbited the Earth for 55 months. In addition to GPS receivers, the satellite carried laser reflectors, a star tracking system, a gradiometer and a drag-free control system.

Figure 3.9: GOCE. *Illustration: European Space Agency (ESA)*

GOCE was the first realization of satellite gravitational gradiometry, hence the on-board gradiometer. A gradiometer is a sensor used to measure change in the acceleration of gravity, i.e. the gravity gradient (Seeber, 2003). When placed on-board a spacecraft, it measures the gravitational gradient. The acceleration of gravity is the first derivative of Earth's gravitational potential, which means a gradiometer measures the second derivative of this potential. The GOCE gradiometer consisted of six accelerometers, placed in pairs on three orthogonal axes, mounted 50 centimetres apart (see figure 3.10). The origin of the orthogonal axes was the satellite's centre of mass. Each accelerometer contained a floating test mass, which was held in place by electrostatic forces. Any deviation of the test mass' position could be directly linked to gravitational forces. Other perturbations could be eliminated by subtracting the observations made by the accelerometer pairs. Due to a relative distance of just 50 centimetres the other perturbation elements were the same for both accelerometers, and disappeared during the subtraction. The result was a gravitational gradient.

Due to GOCE's low altitude, air drag was present and large in magnitude. This is why the satellite had a drag-free control system, which is basically an engine. The engine helped the satellite to stay in a free fall condition, and not to be affected by air drag.

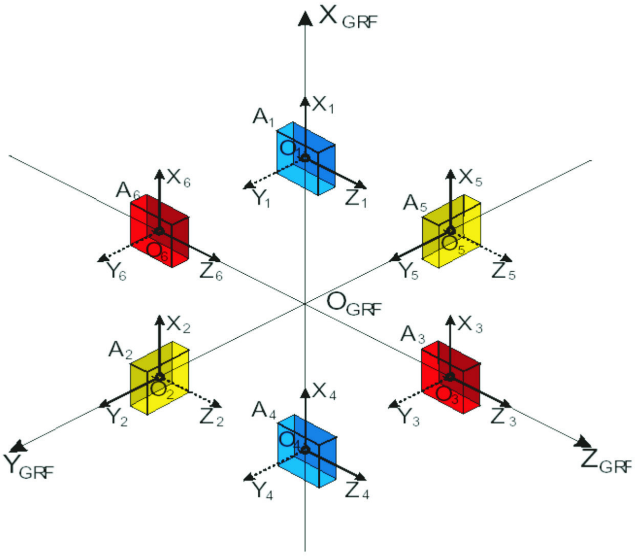

Figure 3.10: Principle of the GOCE gradiometer. *Illustration: European Space Agency (ESA)*

The GOCE mission led to a geoid accuracy of 1-2 centimetres at a spatial resolution of 70 kilometres. The spatial resolution surpassed both CHAMP and GRACE. As GOCE delivered data until fairly recently (October 2013), all the data have yet to be processed, but there is no doubt that it was a successful mission.

3.2.4 The GRACE satellite mission

The Gravity Recovery And Climate Experiment (GRACE) was launched in March 2002, and is a joint project between NASA and the German Space Agency (DLR). The mission was originally intended to last for five year, but GRACE is still operating and is expected to do so until at least 2015 (NASA, 2012). GRACE consists of two identical satellites following each other in the same near-polar orbit (inclination of 89 degrees). With an altitude of approximately 500 kilometres, the two satellites are orbiting 220 kilometres apart, within ± 50 kilometres (Seeber, 2003). Both satellites carry GPS receivers, SLR reflectors, a star tracking system and an accelerometer in the satellite's centre of mass. In addition, a K-band microwave system has been implemented in order to determine their relative distance with an accuracy of 1 micrometer. This means that GRACE is a realization of Satellite-to-Satellite tracking in Low-Low mode.

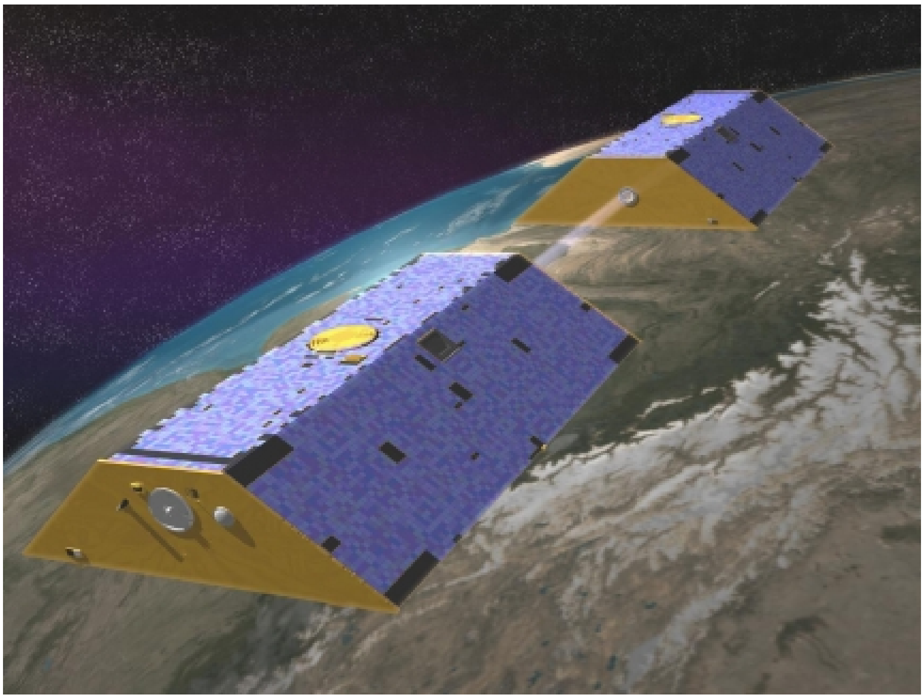

Figure 3.11: GRACE animation. *Illustration: National Aeronautics and Space Administration (NASA)*

When the first satellite passes through a mass anomaly, like a mountainous area, an orbit perturbation occurs. This will propagate into the distance measurement between the two satellites. The distance deviation is then used to derive models of Earth's gravity field. The satellites can very well account for mass anomalies along the satellite orbit, but anomalies placed to the side of the satellite orbit are more difficult to handle (Lysaker, 2011). Similar to CHAMP, GRACE uses accelerometers to account for all non-gravitational accelerations acting on the spacecraft.

Due to an orbit altitude of 500 kilometres, the satellites are able to cover the entire Earth in just 30 days. This paves way for monthly solutions, and deriving temporal variations in Earth's gravity field. The gravity variations studied by GRACE include surface- and deep-water currents in the oceans, variation in ground water storage, mass variation within the Earth and mass variation in ice sheets or glaciers (NASA, 2012). The GRACE satellites are also equipped with engines. This way the operators can extend the mission duration, if they need to, in order to prolong the time series.

3.2.5 Global GRACE gravity models

Several static gravity models from several different developers have been presented since the 1960s by combining satellite data and terrestrial data, as well as using satellite data only. The International Centre for Global Earth Models (ICGEM) is the main distributor of these models.[9] Since the beginning of this millennium, observations from dedicated satellite missions have been implemented. The gravity model EIGEN-1 was the first model where CHAMP data had been included, and it was published in 2002. Then GRACE models came in 2003, and GOCE models became available in 2010. Some static GRACE gravity models are listed below (see table 3.3).

Table 3.3: Some arbitrary examples of static GRACE gravity field models

Model	Degree	Publisher	Published
EIGEN-GRACE01S*	140	GFZ	2003
ITG-Grace03	180	IGG, Bonn university	2007
AIUB-GRACE02S	150	AIUB, Bern university	2009
Tongji-GRACE01	160	Tongji university	2013

**First GRACE model available*

GRACE provide accurate data for the low frequent part of the gravity field. Therefore it is frequently used in hydrological analysis, as well as in mass distribution analysis. The two GRACE satellites only need 30 days to cover the entire Earth with observations, which paves way for monthly GRACE solutions and studies of temporal variations. The monthly gravity field solutions are also distributed by ICGEM, and are developed in different processing centres and institutions. Among them are CSR (University of Texas), GFZ and JPL (California Institute of Technology and NASA). They all have complete solutions from more or less 2003 through 2013.

Due to striping patterns in the monthly GRACE model coefficients, some filtered models are available as well. The applied filter is described in Kusche et al. (2009). The reason for striping patterns and further information on filtering will be discussed in chapter 5 of this thesis.

---

[9] The models can be reached from ICGEM's webpage: `http://icgem.gfz-potsdam.de/ICGEM/`

All the models distributed by ICGEM are available in the ASCII format "gfc", and list a set of spherical harmonic coefficient up to a certain degree and order. The spherical harmonic coefficients can be used in the spherical harmonic synthesis (SHS) to derive anomalies associated with Earth's gravity field.

3.2.6 Comparison of dedicated gravity satellite missions and further outlook

There is no question that the three dedicated gravity satellite missions have played a substantial part in gravity field modelling since the beginning of this millennium. They have all been significant in their own way, and helped us gain a better understanding of Earth's gravity field. CHAMP was the first dedicated gravity satellite, GOCE was the first satellite to realize satellite gradiometry and GRACE provides the best models for studying temporal variations in Earth's gravity field. Table 3.4 shows a comparison of the three satellite missions, to sum up the satellite gravimetry section.

Table 3.4: A comparison of CHAMP, GOCE and GRACE

Properties	CHAMP	GOCE	GRACE
Operator	GFZ	ESA	NASA and DLR
Start of mission	15 Jul 2000	17 Mar 2009	17 Mar 2002
Decay date	19 Sep 2009	11 Nov 2013	Still going
Altitude	300 - 450 km	255 km	500 km
SST mode	High-Low	High-Low	Low-Low
Method	Gravitational perturbations	Gradiometry	Gravitational perturbations
Results	Geoid: 5 cm SR*: ≈400 km	Geoid: 1-2 cm SR*: ≈100 km	Geoid: 1 cm SR*: ≈300 km

**SR = Spatial resolution*

The three satellite missions have been a realization of three different measuring techniques. Figure 3.12 shows an overview of these techniques. Illustration (a) is SST in High-Low mode, as realized through CHAMP. Illustration (b) is SST in Low-Low mode, as realized through GRACE. And finally illustration (c) is SST High-Low mode satellite gradiometry, as realized through GOCE.

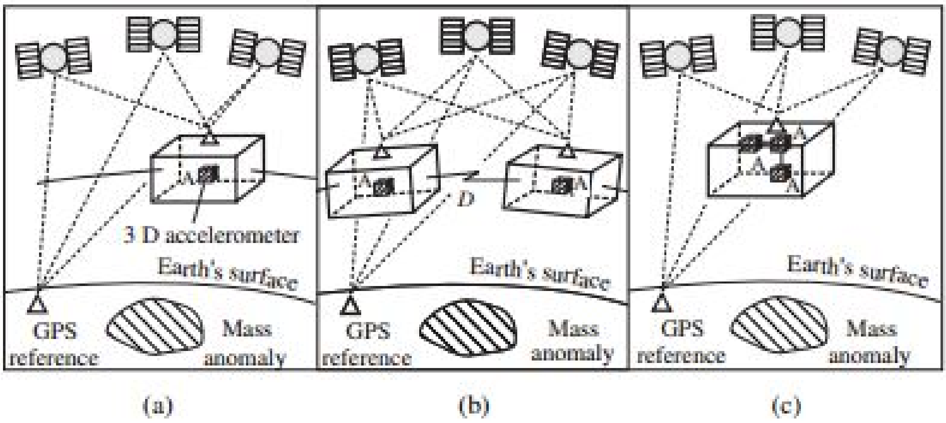

Figure 3.12: Concepts of dedicated gravity field missions. *Illustration: Satellite Geodesy, 2nd edition, page 471 (Seeber, 2003)*

There are some further gravity satellite missions approaching. Simulation studies have been performed and the most promising to be realized is the GRACE follow-on mission with an anticipated launch in 2017. Like the previous GRACE mission, it is a joint project between Germany and USA. The follow-on mission is very similar to the original GRACE mission, but in stead of having a microwave system measuring relative distance between the satellites, a laser ranging instrument has been proposed implemented (Sheard et al., 2012). It may potentially improve the distance accuracy from micrometres to nanometres. However, it also needs to be stated that the most significant limiting factor is the accelerometers.

Chapter 4

Local gravity variations from terrestrial data

The best way of investigating local gravity variations is to use gravimeters, like the ones described in section 3.1. With the accuracy and precision that comes with absolute and superconducting gravimeters, these instruments can be used to detect and describe geophysical phenomena. As established in section 2.3, these are the main causes of temporal gravity field variations.

In this chapter time series of gravity data are analysed. Used to generate the time series are the FG5-226 free fall absolute gravimeter owned by the Norwegian University of Life Sciences (NMBU) and the superconducting gravimeter (SCG) owned by the Norwegian Mapping Authority.

4.1 Description of available data time series

Three different gravity point locations have been chosen when working on this thesis in order to describe local gravity variations. These are the Norwegian University of Life Sciences in Ås and the two stations owned by the Norwegian Mapping Authority in Trysil and in Ny-Ålesund (Svalbard).

Figure 4.1: Geographic location of stations.

The NMBU station has a time series going back to April 2004. This is when the university purchased the FG5-226 free fall absolute gravimeter, and the time series of absolute gravity data began. From 2005 through 2010 this station has been regularly observed. In the years 2011 and 2012 there are some observation gaps, and in 2013 the instrument was in Ny-Ålesund.

The Trysil station was regularly observed in the years 2006 to 2008, and since then some major observation gaps are present. The data from this station is also gathered using the FG5-226.

The Ny-Ålesund station has a continuous time series going back to the late 1990s. The superconducting gravimeter here has been calibrated using absolute gravimeters, including the FG5-226.

4.1.1 Fieldwork in Trysil, Norway

In order to extend the time series in Trysil, Ph.D. candidate Vegard Ophaug, M.Sc. candidate Siri Eikerol and myself travelled to the Trysil station with the instrument FG5-226 in March 2014. Despite some technical difficulties at first, 24 sets of observations over a period of 24 hours were obtained. Each set contained 50 drops.

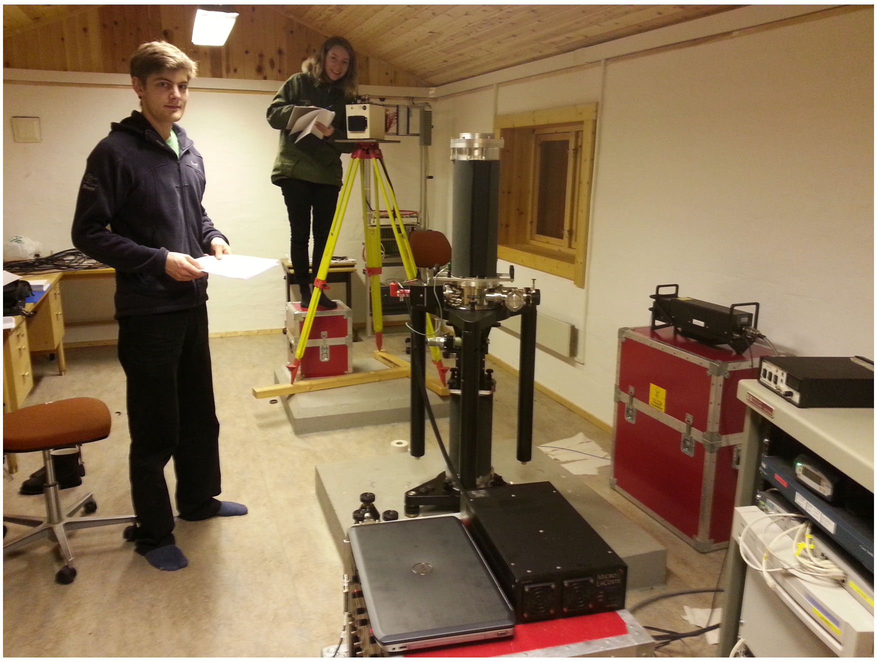

Figure 4.2: Students at work in Trysil. Siri is measuring the gravity gradient, while Vegard assembles the FG5-226.

The obtained result was an absolute gravity value of

$$981827002.47 \pm 1.67 \quad \mu Gal$$

which agreed quite well with former absolute gravity data in Trysil. This result is used in the time series analysis, along with the other Trysil observations, in section 4.3.2.

4.2 Preprocessing

Before using the data in the time series analysis, all the FG5-226 data have been preprocessed. This preprocessing include correction of solid Earth tides, ocean loading, polar motion and barometric pressure. In addition, the rubidium oscillator (atomic clock) had a frequency drift in 2007, which has been accounted for. When correcting for polar motion, the final pole coordinates distributed by the International Earth Rotation and Reference Systems Service (IERS) have been used.

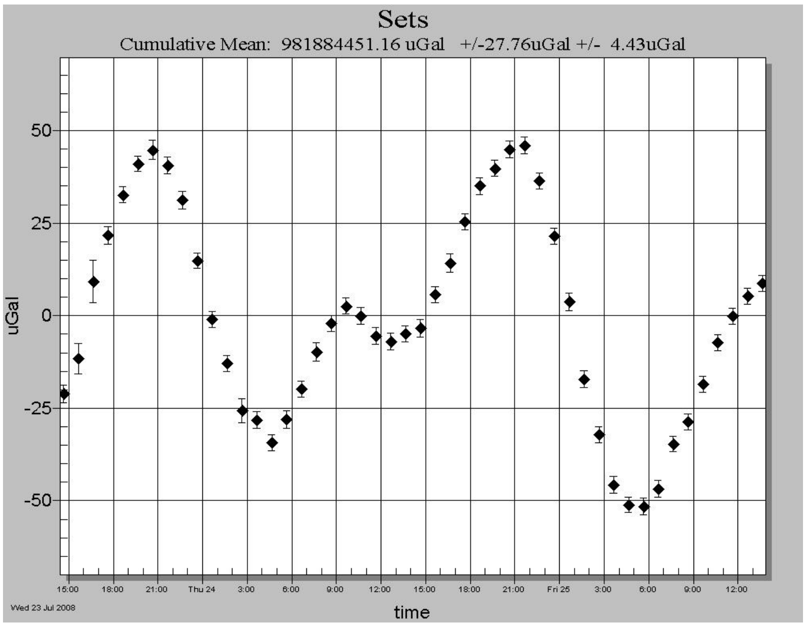

Figure 4.3: 48 hours of FG5 observation, without correction of tidal and loading effects.

If the observations are not corrected by using tide and loading models, the gravity observations will be highly correlated with these geophysical phenomena. In figure 4.3, uncorrected gravity observations from Trysil are displayed. As shown, the gravity value obtained can vary on a 100 microgal interval. If not corrected, the FG5 instrument can be used to monitor these tide and loading effects, but cannot be used as a gravity point value in a gravity network. Nor can it be used to study other geophysical phenomena, such as GIA and near surface mass variations. Gravity observations corrected for tide and loading effects are shown in figure 4.4.

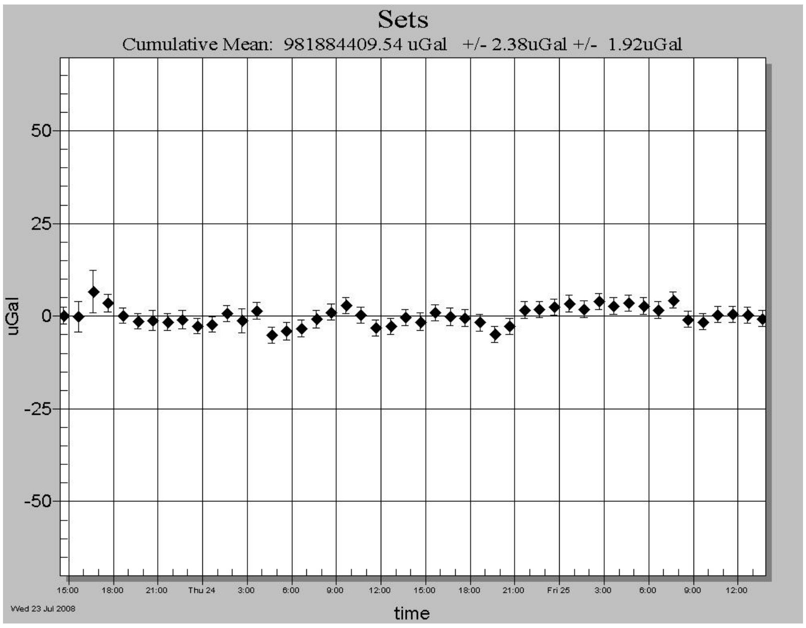

Figure 4.4: 48 hours of FG5 observations, with correction of tidal and loading effects.

4.3 Time series analysis and interpretation

In the following analysis, observations from the three different stations described above are interpreted. All the observations have been preprocessed, as described in section 4.2. The SCG data from Ny-Ålesund have been preprocessed by the Norwegian Mapping Authority.

4.3.1 NMBU, Ås

The Ås region experience GIA at a land uplift rate of approximately 5.1 millimetres per year (Kartverket, 2012). The gravity gradient measured at NMBU reads -0.299 micrograls per millimetre. This means, a decrease in gravity of -1.5 micrograls per year is expected, due to this vertical displacement (see equation 4.1). Like stated in section 2.3.4, GIA also causes a secondary gravity variation effect. A viscous flow in the Earth's mantle, leads to an increase of mass in GIA exposed locations. This secondary effect is proportional to the vertical displacement as shown in equation 4.2 (Wahr et al., 1995).

$$\dot{g}_u = -\frac{2g}{a}\dot{u} \tag{4.1}$$

$$\dot{g}_m \approx \frac{g}{a}\dot{u} \tag{4.2}$$

$$\dot{g} = \dot{g}_u + \dot{g}_m \approx -0.15\ \frac{\mu Gal}{mm}\ \dot{u} \tag{4.3}$$

In the equations above, $\dot{g}$ is the change of gravity with respect to time, $-(2g/a)$ is the gravity gradient and $\dot{u}$ is the vertical displacement with respect to time. Equation 4.3 is from now on referred to as a GIA model in the following analysis. Using the GIA model, which combines both the mass contributor and the vertical displacement contributor, the total expected rate of change in gravity is -0.8 micrograls per year in Ås.

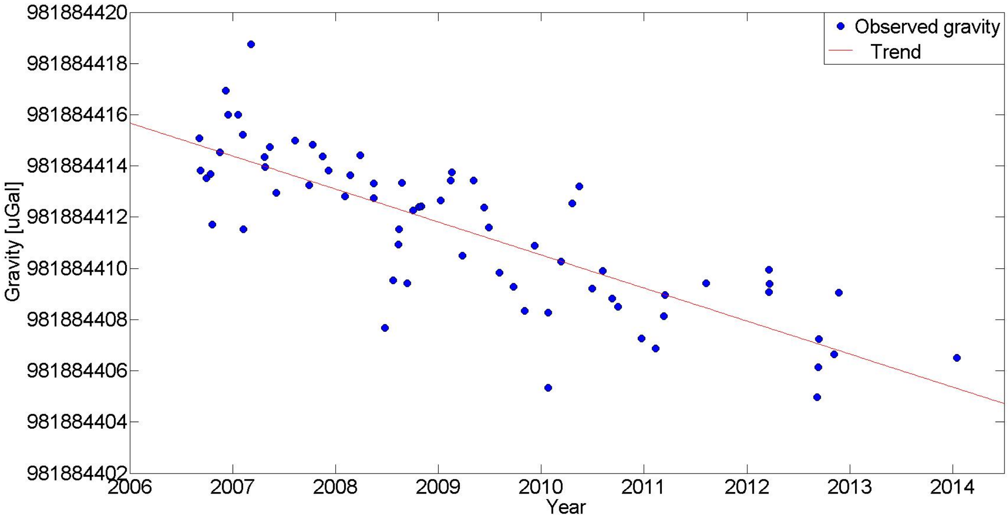

Figure 4.5: Observed gravity from 2006 to 2014 at NMBU.

The negative trend in the gravity observations due to GIA is quite clear in figure 4.5. All observations made between 2006 and present day have been included. The trend was estimated to be -1.3 microgals per year, which deviates from the GIA model of -0.8 microgals per year. The plot shown in figure 4.5 include all observations made between 2006 and present day, which means seasonal variations caused by other geophysical phenomena are present.

Another possibility is to use the linear trend estimate to calculate vertical displacement. By rearranging equation 4.3, it is possible to calculate the annual land uplift by using the FG5 observations. The result is a rate of 8.7 millimetres per year, which differs 3.6 millimetres from the original estimate. This might indicate that the original estimate of 5.1 millimetres per year is a bit low. Although, one must keep in mind that the change in gravity due to mass displacement in equation 4.2 is an approximation.

The NMBU station has a dense dataset of observations between 2007 and 2010. This can be used to estimate seasonal variations in Earth's gravity field on a local scale. As shown in figure 4.6, the seasonal gravity variations at NMBU are small. The absolute gravity values observed vary ± 3 microgals at most, and have an average set scatter of 2.5 microgals for this period. This means that it is difficult to determine seasonal geophysical influence of significant extent.

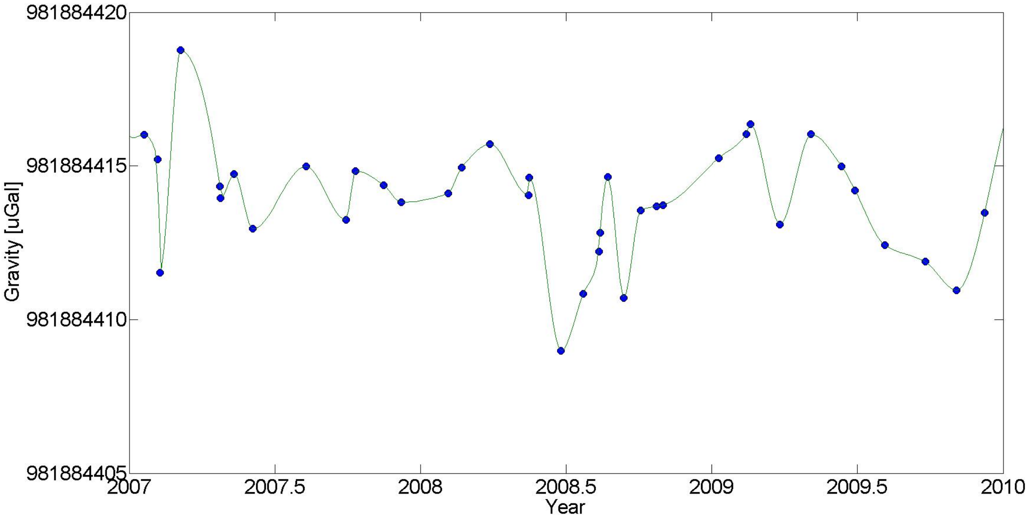

Figure 4.6: Observed gravity from 2007 to 2010 at NMBU. Observations have been corrected for GIA.

4.3.2 Trysil

The Trysil station is placed where Norway experiences the largest effects of GIA. The land uplift rate is approximately 7.7 millimetres per year (Kartverket, 2012). By using the GIA model (equation 4.3), the total expected rate of change is gravity is -1.2 microgals per year.

Like the gravity plot from Ås, the Trysil observations also reveal a clear negative trend. In figure 4.7, all the observations from 2006 and 2014 have been taken into consideration. The estimated rate of change in gravity is -0.9 microgals per year, which deviates from the GIA model. Seasonal variations are present and large in magnitude in Trysil (see figure 4.10), which means a GIA analysis using the plot shown in figure 4.7 is inaccurate.

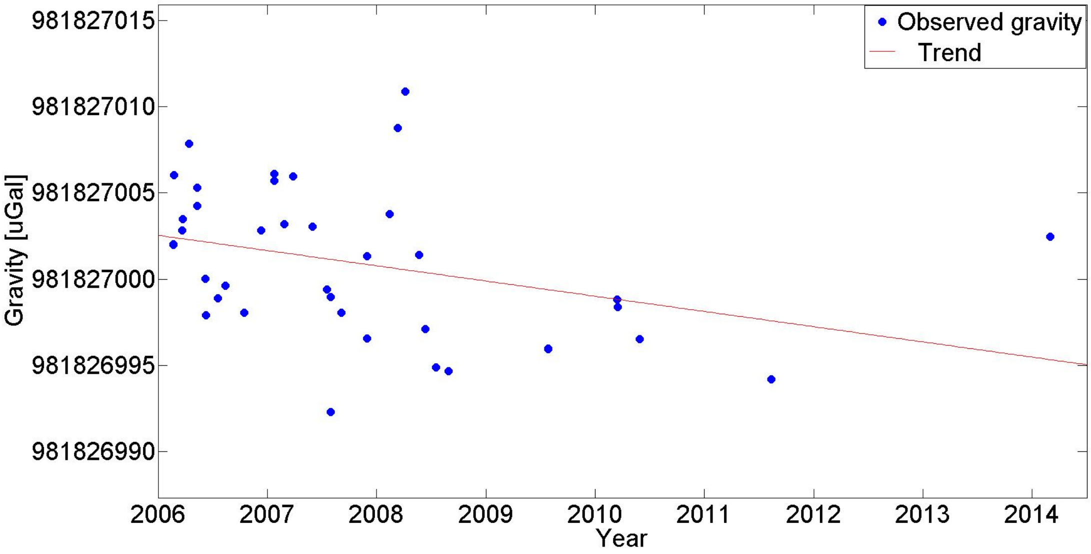

Figure 4.7: Observed gravity from 2006 to 2014 at the Trysil station. All observations between 2006 and present day are included.

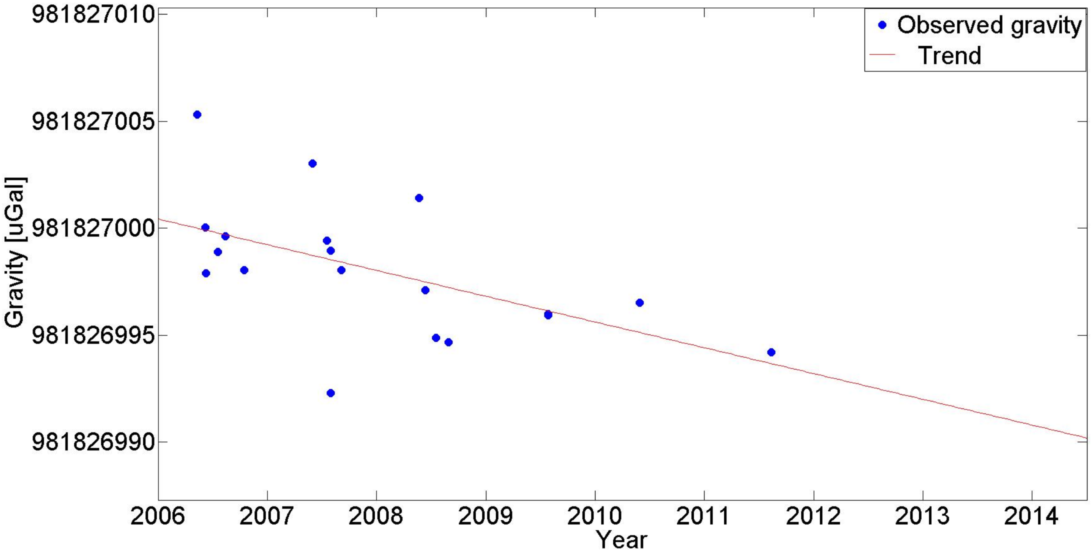

Figure 4.8: Observed gravity from 2006 to 2012 at the Trysil station. Only observations made during the summer months are included.

By removing all the observations gathered during the winter, the seasonal variations in Trysil are less significant (see figure 4.8). The estimated rate of change in gravity, using these observations only, is -1.2 microgals per year. This estimate agrees completely with the GIA model.

If the absolute gravity measurements are used to calculate the rate of land uplift, the result is 8.0 millimetres per year. This differs from the original estimate by the amount of 0.3 millimetres.

The Trysil station has a dense dataset of observations between 2006 and 2009, which can be used to derive seasonal gravity field variations. As shown in figure 4.9, seasonal gravity variations are present to a greater extent in Trysil when compared to NMBU. The observed gravity values vary ± 6 - 8 microgals at most, and the average set scatter for this period is 2.6 microgals.

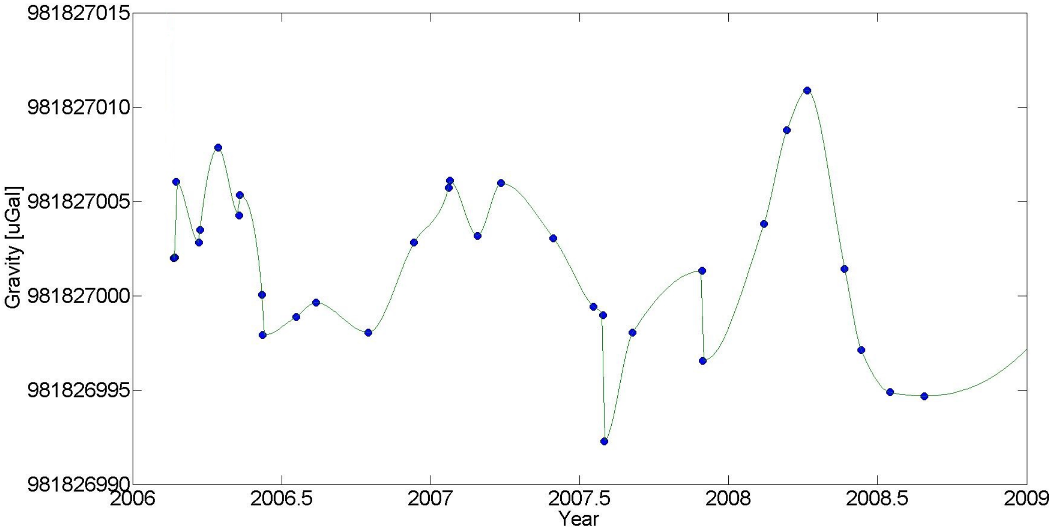

Figure 4.9: Observed gravity from 2006 to 2009 at the Trysil station. Observations have been corrected for GIA.

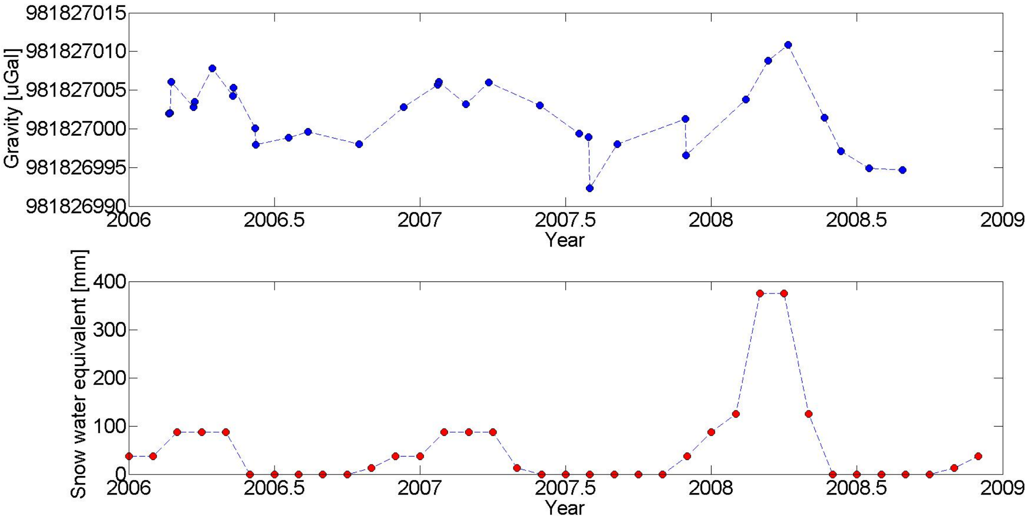

Figure 4.10: Gravity variation compared to snow water equivalent.

The gravity variations can be explained by local hydrological variations. Trysil gets covered by significant amounts of snow every year. This is resulting in an increased gravity value, as all the snow is located below the Trysil station. Figure 4.10 displays a comparison of gravity variation and variation in snow water equivalent (SWE).[1] The SWE data have been gathered by the Norwegian Water Resource and Energy Directorate, and distributed from www.senorge.no. As observed in this figure, there is a significant correlation between gravity value and SWE estimate. This means that local gravity variations in Trysil are directly dependent on the amount of snow. In addition, there is a secondary effect as all snow and precipitation in general will result in groundwater variations.

4.3.3 Ny-Ålesund

The land uplift in Ny-Ålesund, Svalbard, is a bit more complex compared to the Norwegian mainland. In addition to GIA, there is a local land uplift due to the ongoing ice melting Svalbard experience today. The total land uplift is approximately 8.5 millimetres. However, the land uplift rate can vary over 10 millimetres from year to year (Kierulf, 2012). An average land uplift rate of 8.5

---

[1] Snow water equivalent is an estimate of how much water the snow would correspond to if melted.

millimetres, corresponds to a total annual decrease in gravity of -1.3 microgals per year. This is the result when using the GIA model described in equation 4.3.

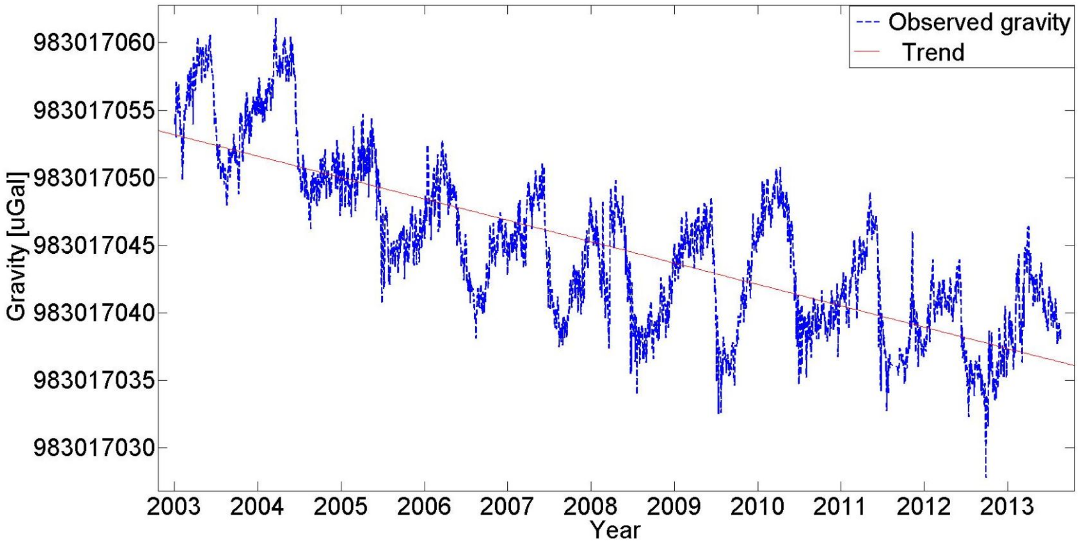

Figure 4.11: Observed gravity from 2003 to 2013 in Ny-Ålesund. All the observations are made by the superconducting gravimeter, and have been calibrated using absolute gravimeters in the period 2003 to 2010.

There is a clear negative trend in the SCG observations, indicating that land uplift is present (see figure 4.11). There is also a distinct amount of seasonal variations observable. However, since the SCG instrument has a continuous time series, the seasonal variations cancel each other out when applying a linear fit. It can be observed that the gravity curve deflects more from the linear trend when compared to the observations carried out in Trysil and at NMBU. This is indicating that the land uplift rate has annual variations, like stated by Kierulf (2012) and Omang and Kierulf (2011).

The estimated annual change in gravity in this period was -1.6 microgals per year, which agrees quite well with the combined GIA and local land uplift model. If the SCG observations are corrected for the land uplift rate, the observations can be used to study seasonal gravity variations (see figure 4.12)).

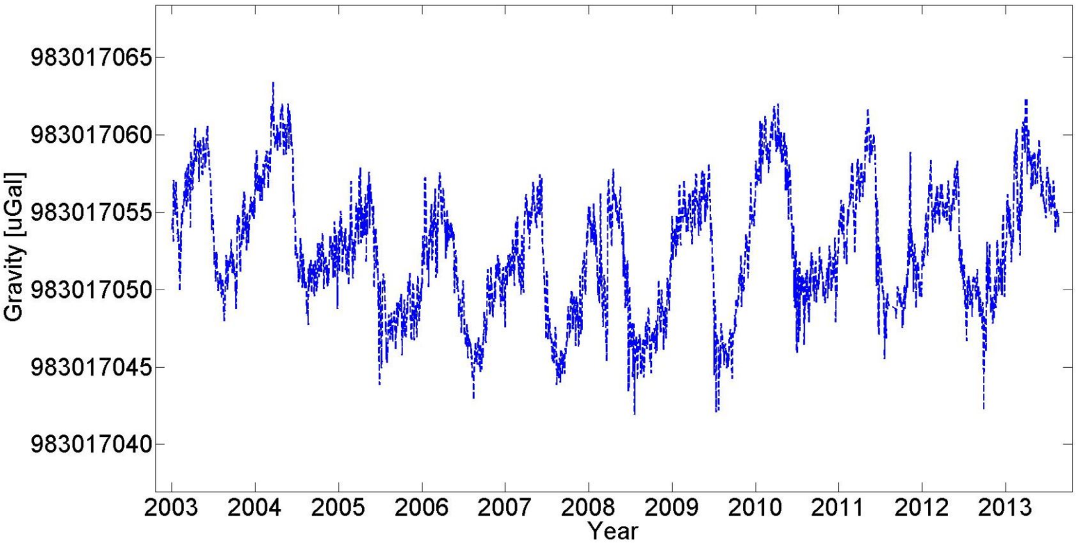

Figure 4.12: Observed gravity from 2003 to 2013 in Ny-Ålesund. The observations have been corrected for GIA and local land uplift.

The semi-annual variation is of the order ± 8 - 9 microgals at most. The gravity peaks around January - March each year and is at its lowest around July - September each year. This is highly correlated with the seasonal variations in weather and precipitation. These results indicate that hydrological variation is the major cause of seasonal gravity variations in Ny-Ålesund.

Table 4.1: GIA analysis

Station	Period	GIA model	$\dot{g}$	$\dot{u}$
NMBU	2006 - 2014	-0.8 $\frac{\mu Gal}{yr}$	-1.3 $\frac{\mu Gal}{yr}$	8.7 $\frac{mm}{yr}$
Trysil	2006 - 2011	-1.2 $\frac{\mu Gal}{yr}$	-1.2 $\frac{\mu Gal}{yr}$	8.0 $\frac{mm}{yr}$
Ny-Ålesund	2003 - 2014	-1.3 $\frac{\mu Gal}{yr}$	-1.6 $\frac{\mu Gal}{yr}$	10.7 $\frac{mm}{yr}$

A comparison of GIA results from the three different stations is given in table 4.1. For the NMBU and the Ny-Ålesund stations, all observations have been taken into consideration. In Trysil, only the observations made during the summer months have been included.

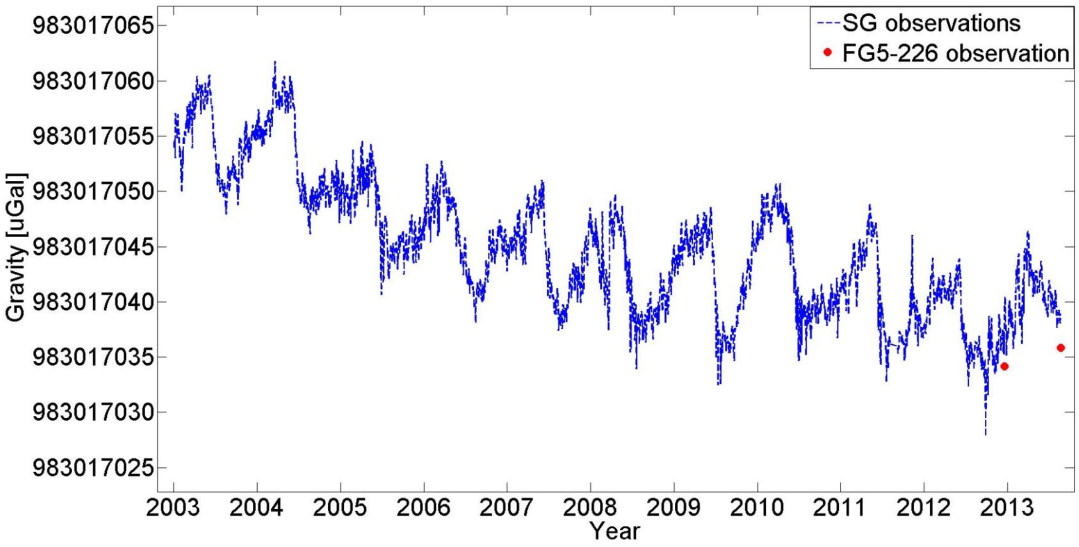

Figure 4.13: The SCG time series in Ny-Ålesund compared to two single FG5-226 observations.

In figure 4.13, a comparison of the SCG time series and two single FG5-226 observations is given. There is a small deviation present (1 - 3 microgals), which might indicate that the SCG time series has drifted a bit since last calibrated in 2010.

Chapter 5

Global gravity field variations from GRACE

Since the launch in 2002, GRACE has provided observations that have led to monthly gravity field solutions on a global scale. With its 300 kilometres spatial resolution, local gravity field variations are difficult to derive from GRACE data. This chapter describes how to compute global gravity field variations, using GRACE data in a spherical harmonic synthesis.

5.1 Data reduction and de-aliasing

The official GRACE products are categorized into four different levels. These are Level 0, Level 1A, Level 1B and Level 2. A short description of each level is given in this section.

GRACE cannot resolve short periodic mass variations (atmosphere and ocean). This would create aliasing if not accounted for computationally. Therefore, these effects are modelled in order to reduce the observations before analysed. This process is known as de-aliasing.

5.1.1 Level 0

Level 0 data include observational raw data, and are processed by the GRACE Raw Data Center (RDC) at DLR in Neutstrelitz (Case et al., 2002). From each downlink pass, two files including raw data are made available and kept in the archives at RDC. These files are known as the GRACE Level 0 data products.

5.1.2 Level 1A

When a non-destructive processing have been applied to the Level 0 data, the Level 1A data emerge. The processing include a sensor calibration, ambiguity resolving and reformation of data (Case et al., 2002). The sensor calibration has to be carried out in order to convert the raw data from binary encoded measurements into engineering units. The Level 1A data can be reversed into Level 0 data.

5.1.3 Level 1B

By correctly time-tagging the Level 1A data, the Level 1B data emerge. In addition, the data sample rate is reduced. The Level 1B data are made available when the monthly gravity field solutions are delivered to the science community (Case et al., 2002).

5.1.4 Level 2

The final level is Level 2. These products have been de-aliased and are available as spherical harmonic coefficients. The Level 2 data also include the GRACE orbits. These models are made available within 60 days of acquisition (Case et al., 2002).

5.2 Estimation of annual and semi-annual variations

When potential models have been categorized as Level 2 products, it is possible to derive annual and semi-annual variations. These variations become visible in geoid variation maps. Geoid variation maps can be generated using different methods. One of the methods is averaging over all the monthly solutions in the time series of interest, and then subtracting the average from each monthly solution. Another method is to choose a reference geoid from one monthly solution, and subtract this reference geoid from the other monthly solutions. Both methods are used in this analysis.

From a sequence of monthly GRACE solutions, a time series for each of the spherical harmonic coefficients is set up. This time series is analysed for linear and quadratic trends, as well as for periodic components. This analysis is carried out using the model shown in equation 5.1 in a weighted least square fitting.

$$C_{nm}(t) = C_{nm}(t_0)+a(t-t_0)+\frac{1}{2}b(t-t_0)^2+A\cos[\omega(t-t_0)+\phi_A]+S\cos[2\omega(t-t_0)+\phi_S] \tag{5.1}$$

The corresponding trend, annual and semi-annual coefficients can be estimated using the following equations.[1]

$$C_{trend} = C_{nm}(t_0) + a(t-t_0) \tag{5.2}$$

$$C_{annual} = C_{nm}(t_0) + A_1\sin(\omega(t-t_0)) + A_2\cos(\omega(t-t_0)) \tag{5.3}$$

$$C_{semi-annual} = C_{nm}(t_0) + S_1\sin(2\omega(t-t_0)) + S_2\cos(2\omega(t-t_0)) \tag{5.4}$$

---

[1] The same equations hold for both C_{nm} and S_{nm} coefficients.

5.2.1 Statistical properties of monthly GRACE solutions

All the monthly solutions used in this analysis are complete to spherical harmonic degree and order 90. In this section, the statistical properties of the time variable GRACE field from July 2013 are given.

As shown in figure 5.1, the theoretical degree variance model Kaula coincides with the degree variacne curve plotted from the monthly GRACE solution. Two error degree variance curves have been plotted as well in figure 5.1. These are both a description of the error degree variance from the same monthly solution (July 2013). However, the cyan-coloured curve is from an unfiltered potential model and the green-coloured is from a filtered potential model. When applying a low-pass filter, like the one applied here,[2] the high frequencies are down-weighted.

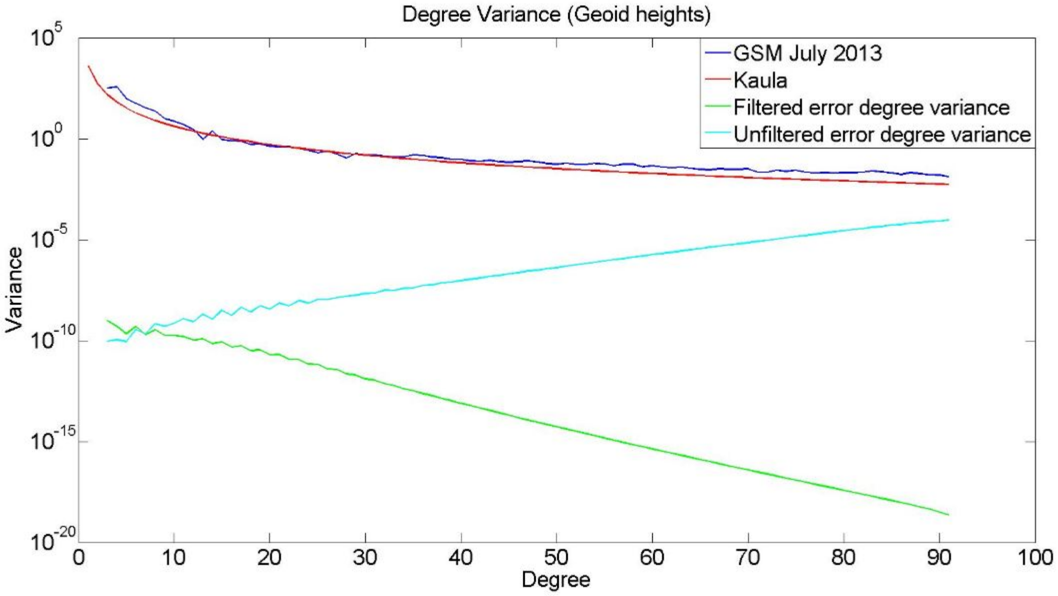

Figure 5.1: Degree variance plot of a monthly GRACE solution.

Commission-, omission- and total errors have been calculated using both models, and the results are shown in table 5.1. Since both models are complete to degree and order 90, the omission errors are the same for both models. The commission errors, however, are different. Since the filtered model have down-weighted high frequent errors, the commission error will be smaller in magnitude when compared to the unfiltered model.

---

[2] The filter used is as described in Kusche et al. (2009).

Table 5.1: Error analysis

Model	Commission error [m]	Omission error [m]	Total error [m]
Unfiltered model	0.03	0.50	0.50
Filtered model	0.00	0.50	0.50

5.3 Filtering of spherical harmonic models

The most difficult problem faced when analysing GRACE data is correlated errors. These are present in the higher degrees in the model coefficients, when attempting to derive gravity field variations. The errors show up as longitudinal striping patterns in geoid maps and in surface mass anomaly maps. The cause of these correlated errors are most likely due to the satellite orbit geometry (Ray and Luthcke, 2006). The two GRACE satellites are measuring their relative distance, as they orbit the Earth in a near-polar orbit. As previously stated in chapter 3, the GRACE satellites are highly sensitive for gravity field variations in the along-track direction. Instrument and background model errors will consequently result in a spatial correlation (Wouters, 2010).

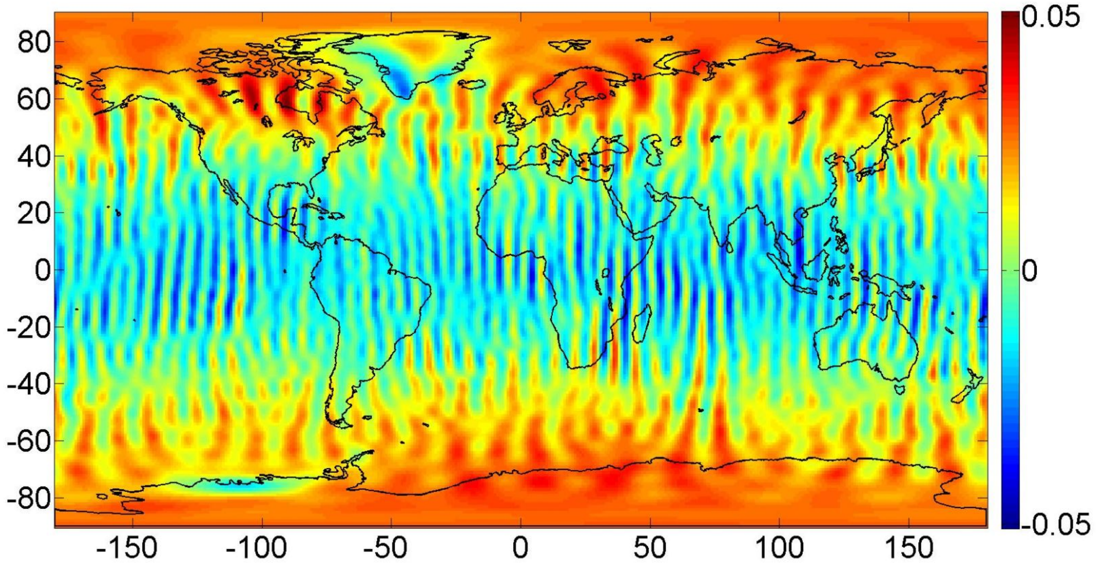

Figure 5.2: Unfiltered monthly GRACE solution in terms of geoid height [m].

Displayed in figure 5.2 is the monthly solution from January 2013, provided by GFZ. In order to derive gravity field variations, the monthly solution from January 2003 has been used as reference. This model is also provided by GFZ. All the spherical harmonic degrees up to degree 60 have been included. The striping pattern is very visible in this figure, and little to no information can be retrieved from the model. The striping pattern is most dominant between latitudes 60S and 60N. This is due to near-parallel orbits by the equator. Also, GRACE makes more observations near the poles. In addition to the striping pattern, there are some systematic errors present as well. These can be observed as homogeneously red areas near the poles, and a more green/blue area between latitudes 40S and 40N. These errors are due to GRACE's uncertainty at low spherical harmonic degrees. This means that the coefficient errors will be dominant when deriving gravity field variations. To deal with this issue, it is often preferable to start at degree 2 - 5 when analysing GRACE data. Another possibility is simply to replace the lowest coefficients with SLR data.

The correlated errors increase above the spherical harmonic degree of about 10. One proposed solution to remove this correlation effect has been to only include model coefficients up to this degree. This will limit the model resolution significantly, and the method is hence not preferable. Instead, advanced filtering techniques have been implemented in order to reduce the correlation effects. Some of which will be given an introduction in the following sections.

5.3.1 Gaussian smoothing

Noise reduction in GRACE data, using a spatial averaging method, was first proposed by Wahr et al. (1998). The most frequently used smoothing kernel in GRACE analysis is the Gaussian bell shaped kernel (Wouters, 2010). This method use a weighting factor (W) in order to down weight and reduce the noise in higher spherical harmonic degrees. The weighting factor is only depending on the distance from computation points, and not the orientation, making Gaussian smoothing an isotropic method. The weighting function can be calculated using

$$W(\alpha) = \frac{Be^{-B(1-\cos(\alpha))}}{2\pi(1-e^{-2B})} \tag{5.5}$$

$$B = \frac{\ln 2}{1-\cos(\frac{r}{a_e})} \tag{5.6}$$

where a_e is mean equatorial distance, r is the kernel radius and α is the distance of interest point to the centre of the kernel. The values of the weighting factors can also be approximated using the numerical method proposed by Chambers (2006). The weighting function *W(n)* can then be calculated using

$$W(n) = \exp\left(\frac{\left(\frac{nr}{2a_e}\right)^2}{\ln 2}\right) \tag{5.7}$$

where n is spherical harmonic degree. The weighting function can further be implemented in the spherical harmonic synthesis as shown in equation 5.8.

$$V(r,\theta,\lambda) = \frac{GM}{R}\sum_{n=0}^{\infty}\left(\frac{R}{r}\right)^{n+1} W_n \sum_{m=0}^{n} P_{nm}(\cos\theta)[C_{nm}\cos(m\lambda) + S_{nm}\sin(m\lambda)] \tag{5.8}$$

A Gaussian filter is isotropic. The correlated errors, on the other hand, is of non-isotropic character. In order to remove all the correlated errors, the Gaussian smoothing radius has to be large. A large smoothing radius will compromise some of the information GRACE provides, which means that a Gaussian filter alone is not always the best solution.

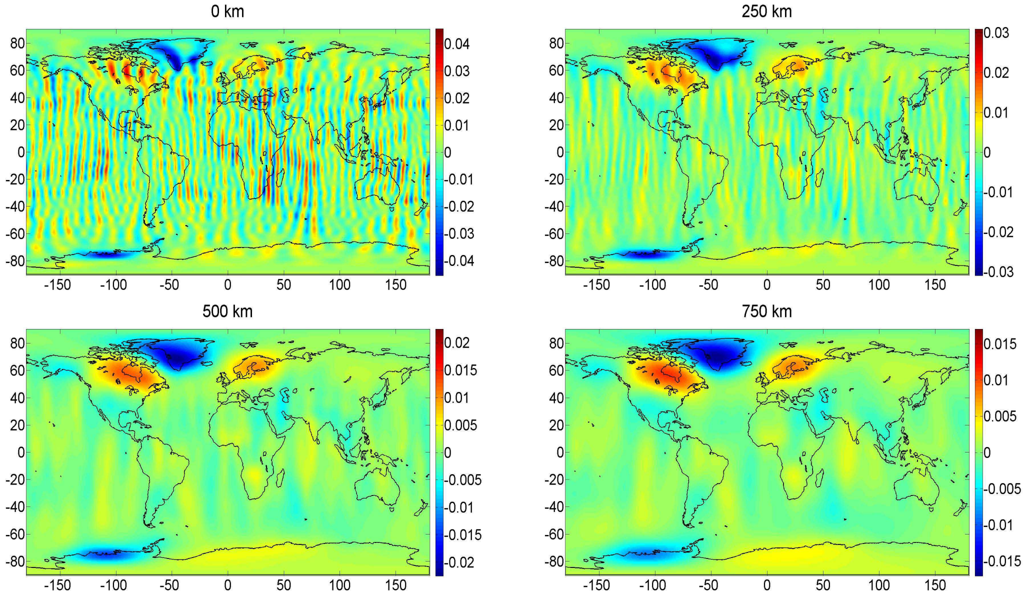

Figure 5.3: Displayed are the effects of Gaussian filters with different smoothing radii in a geoid height map [m].

Figure 5.3 displays the same monthly solution as the one shown in figure 5.2, only this time the spherical harmonic degrees between 0 and 4 have been excluded in order to reduce the systematic errors. The same monthly solution has been used as reference. The upper left image displays the monthly solution as it is, i.e. no Gaussian smoothing has been applied. The image is dominated by noise, and no information can be retrieved. The model in the upper right image has been inflicted by a Gaussian filter with a smoothing radius of 250 kilometres. It is now possible to observe some gravity field variations, but there is still a lot of noise remaining. The two bottom images have gone through a filter with smoothing radius of 500 and 750 kilometres. In both images it is possible to observe gravity field variations, like GIA and ice melting. The corresponding weighting functions are shown in figure 5.4.

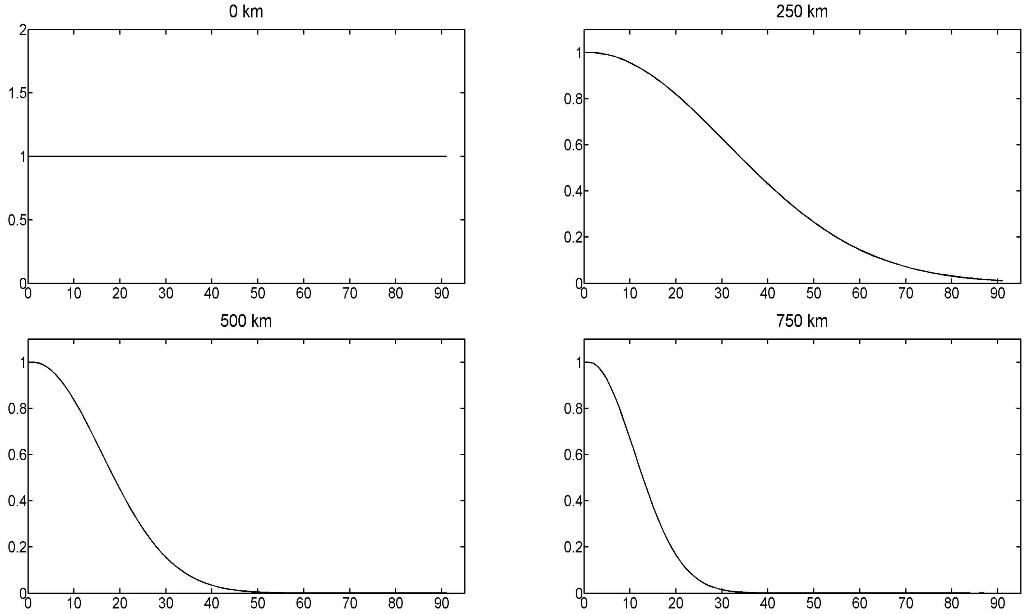

Figure 5.4: Weight as a function of spherical harmonic degree.

Figure 5.4 shows the weight factor as a function of spherical harmonic degree when different filters have been applied. Although the models have been computed using up to degree and order 60, the weight factor goes to zero before reaching degree 60 in the two bottom graphs. The weighting function can be used as an indicator of how much model information is lost when applying different filters.

5.3.2 Non-isotropic smoothing

Gaussian smoothing has been the standard filtering method used in the early GRACE analysis. However today, other decorrelation methods have been proposed. These methods are often used in conjunction with Gaussian smoothing. The whole purpose of non-isotropic smoothing is to decorrelate the GRACE solutions, without compromising the data provided by GRACE.

ICGEM distributes filtered monthly solutions, as well as unfiltered solutions. The used filter is as described in Kusche et al. (2009). The basic principle of this filter is to use an a priori synthetic model of the observation geometry. This is resulting in a non-symmetric axes system, making it a non-isotropic filter.

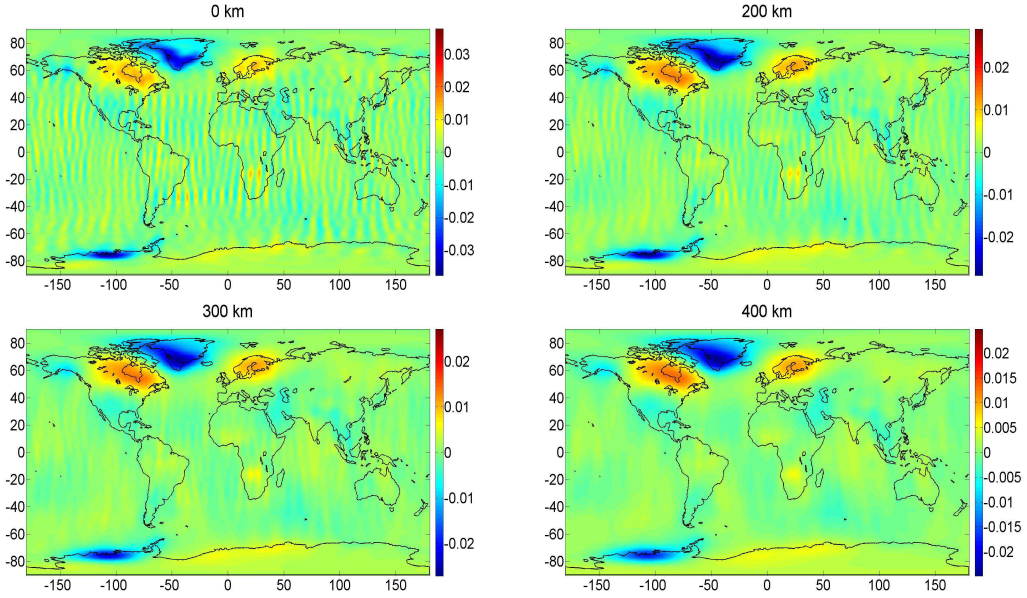

Figure 5.5: A conjunction of Kusche-filtered model and Gaussian smoothing, displayed in a geoid height map [m].

In figure 5.5, a Kusche-filtered monthly solution from GFZ is shown. Even when no Gaussian smoothing have been applied, it is possible to observe gravity field variations. However, there are some remaining correlated errors in the upper left image. In the three other images the Gaussian smoothing has eliminated the majority of the correlated errors quite effectively. This by using a smaller smoothing radius than the ones used in figure 5.3. This supports the statement that a non-isotropic smoothing approach preserves the GRACE information more than an isotropic smoothing approach.

One final non-isotropic smoothing approach is empirical orthogonal function (EOF) analysis. This method corresponds to principal component analysis (PCA). The basic principle is to separate the directions of the largest variance from each other (Wouters, 2010). By doing this, the GRACE data can be transformed to a reduced subspace with a lower number of directions. This method was first used by Chambers (2006) to filter GRACE data, in order to minimize the loss of information.

5.4 Time series analysis and interpretation

Kusche-filtered monthly solutions from GFZ Release 05 have been used in the following time series analysis.[3] Due to the uncertainty in the lower spherical harmonic degree, the synthesis has been carried out using n = 5 : 90. This means that the absolute geoid variation in terms of number of meters is not available in the following geoid maps.

5.4.1 Global gravity field variations covering several years

Global gravity field variations in July 2013 with respect to January 2003 are shown in figure 5.6. The geoid variation map has been computed using the trend coefficients, which means seasonal variations have been eliminated. No Gaussian smoothing was needed, as the trend signal is not correlated with the striping pattern. The gravity field trends are dominated by GIA and ice melting.

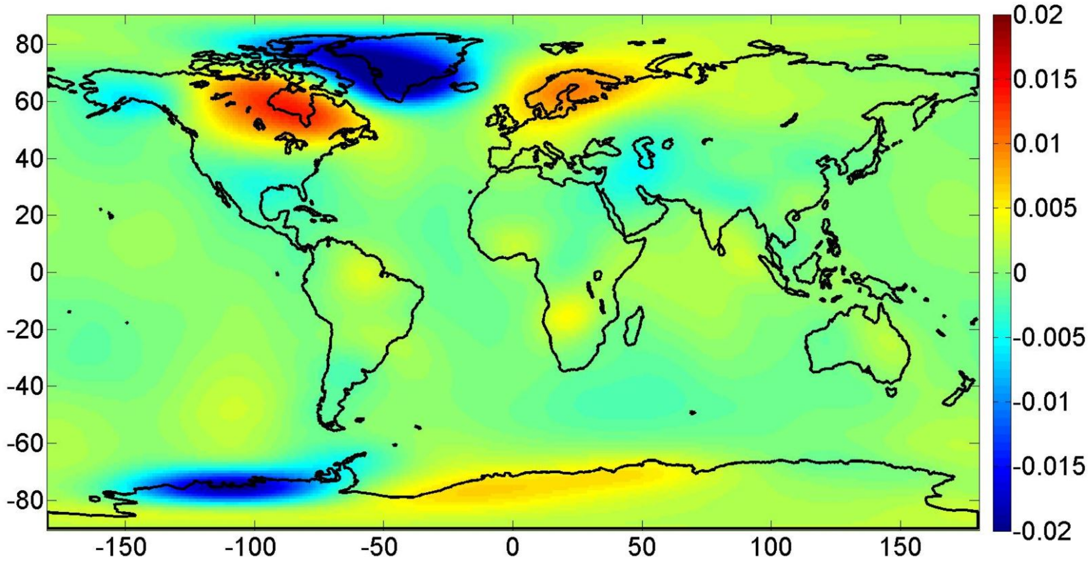

Figure 5.6: Gravity field variations from January 2003 to July 2013 displayed in terms of geoid variation [m].

---

[3] ICGEM distributes three different Kusche-filtered models. Used in this analysis is the DDK1 filter.

Due to the massive storage of water as land-covering ice during the last glacial period (see section 2.3.4), GIA is observable in the northern parts of North-America, Fennoscandia and Antarctica today. The GIA shows up as orange and red areas in figure 5.6, indicating a mass increase in these regions. Even though Antarctica is still covered by ice today, the region experience GIA. The land-covering ice masses formed during the last glacial period are much greater in magnitude than the ice masses found in Antarctica today. This is resulting in a decrease of pressure on Earth's crust, leading to this land uplift.

The change in the Earth's cryosphere can be found in Greenland and West-Antarctica, as well as some changes in Alaska. This effect shows up as blue and dark blue areas in figure 5.6, and indicate a loss of mass in these regions. The mass displacement is caused by ice melting, due to the rise in average temperature of Earth's climate system (see section 2.3.5).

5.4.2 Seasonal gravity field variations

In the following analysis, an attempt to observe seasonal gravity field variations have been carried out. GRACE data from 2006 to 2009 have been used. These years have been chosen on the basis that there are no observational gaps in this period. However more importantly, these are the years with the most dense dataset of terrestrial gravimetry observations. In chapter 6, there is an attempt to compare satellite-only GRACE data with point wise terrestrial data. This timespan is hence of most interest in this thesis.

Long term trends have been eliminated from the data used in this analysis. To derive geoid variation maps, an averaged mean field from each year has been subtracted from every monthly solution.

Global approach

As long term trends are excluded, GIA and ice melting on the large ice sheets are not expected to be observed in the following analysis. The dominant geophysical phenomena in seasonal gravity field variations is hydrological variations. The analysis in this section have been carried out using the annual coefficients (see equation 5.3).

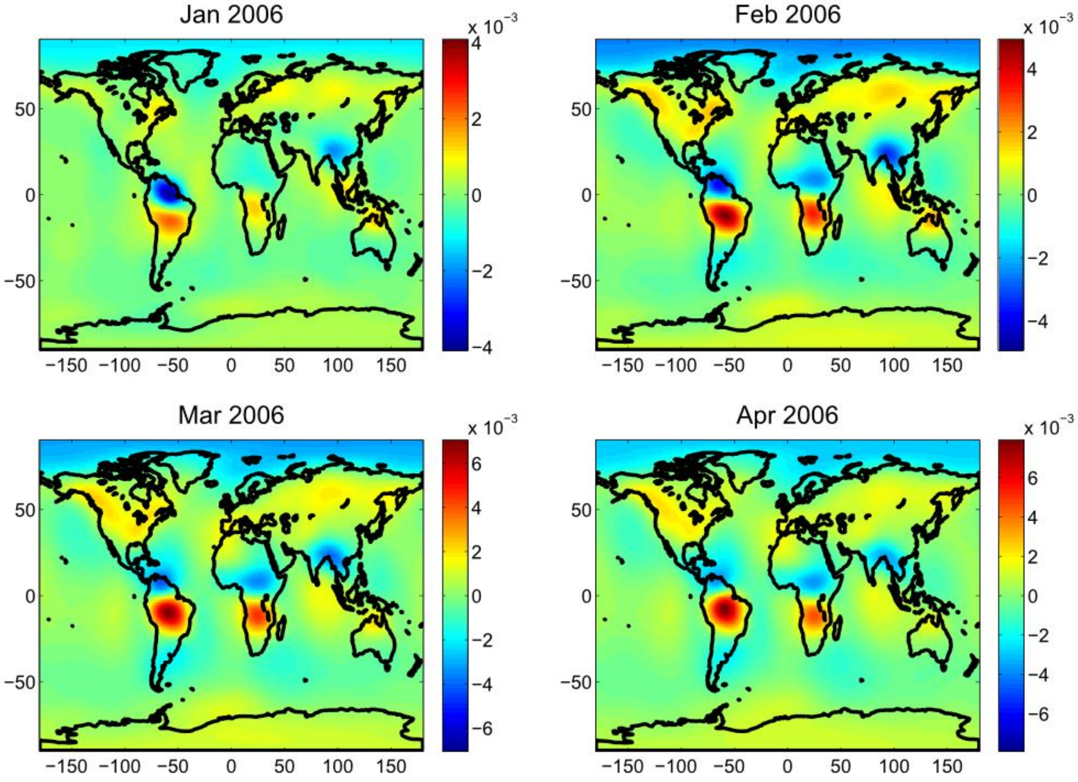

Figure 5.7: Seasonal gravity field variations in terms of geoid variation [m]. January - April, 2006.

The first thing that draws attention in figures 5.7, 5.8 and 5.9 is the dark blue or dark red colours that cover the Amazon. The climate in the Amazon rainforest is divided into a wet season and a dry season.[4] The wet season last from December to May, and the dry season last from June to November (Marengo et al., 2001). This is in agreement with the geoid variation maps displayed in figures 5.7, 5.8 and 5.9. A dominant red coloured area covering the Amazon in the months January to June is observable, indicating a mass increase in this period. From July to December, a blue coloured area is covering the Amazon, indicating the opposite. This change in the hydrological cycle can be explained by groundwater variations, as groundwater is very weather and precipitation dependent.

The same seasonal variations can be found in the southern parts of Africa. The wet season, from November to April, are visible in the geoid variation map as a

---

[4] Since the Amazon is a rainforest, it experience rain through the whole year. But the amount of precipitation varies a lot between seasons.

positive mass anomaly. The dry season, from May to October, can be seen as a negative mass anomaly.

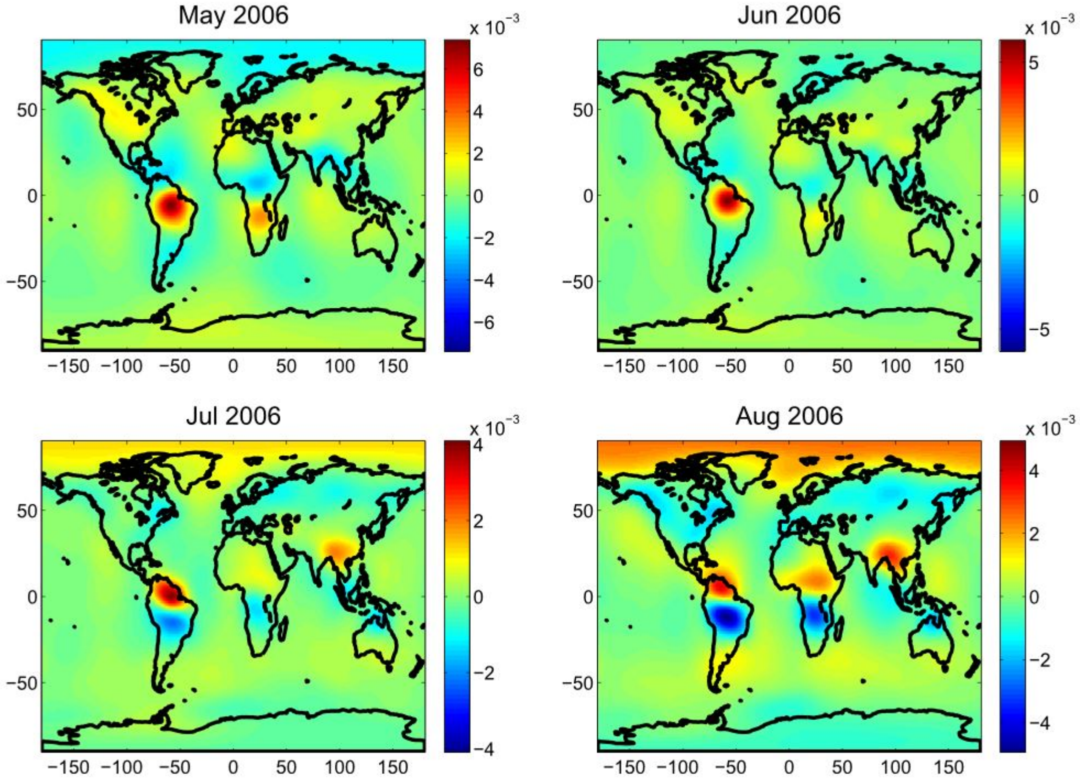

Figure 5.8: Seasonal gravity field variations in terms of geoid variation [m]. May - August, 2006.

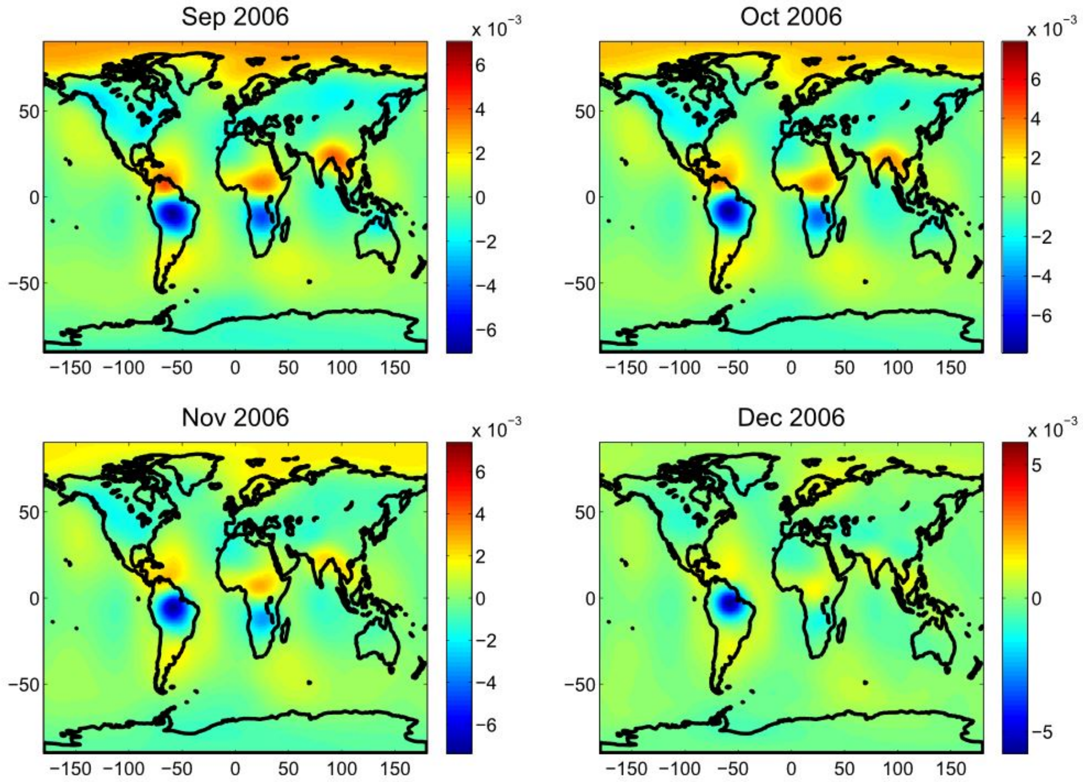
Sep 2006

Oct 2006

Nov 2006

Dec 2006

Figure 5.9: Seasonal gravity field variations in terms of geoid variation [m]. September - December, 2006.

The seasonal variations found in the gravity field variation analysis from 2007 to 2009 agree very well with the 2006 analysis (see appendix A). This indicate that the seasonal variations do not change in the timespan 2006 to 2009, and are mostly due to hydrological variations.

Chapter 6

Comparison of terrestrial and satellite based gravity variations

There is one fundamental difference between terrestrial and satellite gravimetry, which has to be taken into account when attempting to compare the two measuring techniques. Terrestrial gravimeters measure gravity in Earth's gravity field and satellites observe gravitation in Earth's gravitational field. Gravity include the centripetal acceleration, as well as gravitation. The effect of the Earth's rotation is 0.3 percent of the gravity at the equator (Breili, 2011).

As satellites are only exposed to gravitational effects,[1] geometric effects like GIA induced vertical displacement cannot be observed by satellites like GRACE. A ground based gravimeter, however, observe both gravitational effects and geometric effects.

Terrestrial observations generate a gravity point value, whereas GRACE generate a surface with one averaged gravity value. GRACE's footprint is approximately 300 kilometres. Therefore, it is not straightforward comparing terrestrial gravimetry data with GRACE. However, in this chapter studies have been performed to see if GRACE and terrestrial gravimetry can detect some of the same geophysical signals in Earth's gravity field on a local scale.

---

[1] Gravitational effects include mass effects and third-body effects.

6.1 Local approach

The observational material used in this chapter is more or less the same as in chapter 4 and chapter 5. Used are the GRACE monthly solutions from 2003 to 2013, terrestrial FG5 data from 2006 to 2014 and SCG data from 2003 to 2013.

Comparison of terrestrial gravimetry data and space based data can be carried out using different methods. One of the most common methods is to use terrestrial data gathered from several different stations to generate a gravity surface. In other words, adjust the terrestrial gravimetry data to fit GRACE data. This, however, presupposes that a dense terrestrial gravity network is available in order to achieve an optimal foundation for comparison. Another method, used in this chapter, is to make GRACE data fit terrestrial gravimetry data.

6.1.1 Method

Through the spherical harmonic synthesis, it is possible to calculate point values from GRACE, instead of global or regional grids. This is an attempt to generate a GRACE based observation material that can be used in comparison with terrestrial point data. The point value generated from GRACE, however, has a correlation radius of 300 kilometres. This means that the gravity signal will be the same for Trysil station and the NMBU station, as these are only 200 kilometres apart. The distance from Earth's centre of mass varies between the two positions, which means that the calculated gravity values will differ.

By using the equations 2.22, 2.23 and 2.24, it is possible to approximate an absolute gravity value from the potential coefficients. All the spherical harmonic degrees (n = 0 : 90) have been included in the monthly solutions in this following analysis. Since all the spherical harmonic degrees available have been included, the Dynamical Form Factor (C_{20}) has been replaced by SLR observations.

In addition to mass variation, hydrological variations cause a crustal deformation, leading to vertical displacement. This effect can be taken into account by using degree dependent load love numbers in the spherical harmonic synthesis (Neumeyer et al., 2008). The load love numbers are parameters describing the sensitivity of the solid Earth to loading effects.

6.2 Time series analysis and interpretation

Kusche-filtered monthly solutions from GFZ Release 05 have been used in the following time series analysis. All the terrestrial observations have been preprocessed, as described in section 4.2. The SCG data from Ny-Ålesund have been preprocessed by the Norwegian Mapping Authority.

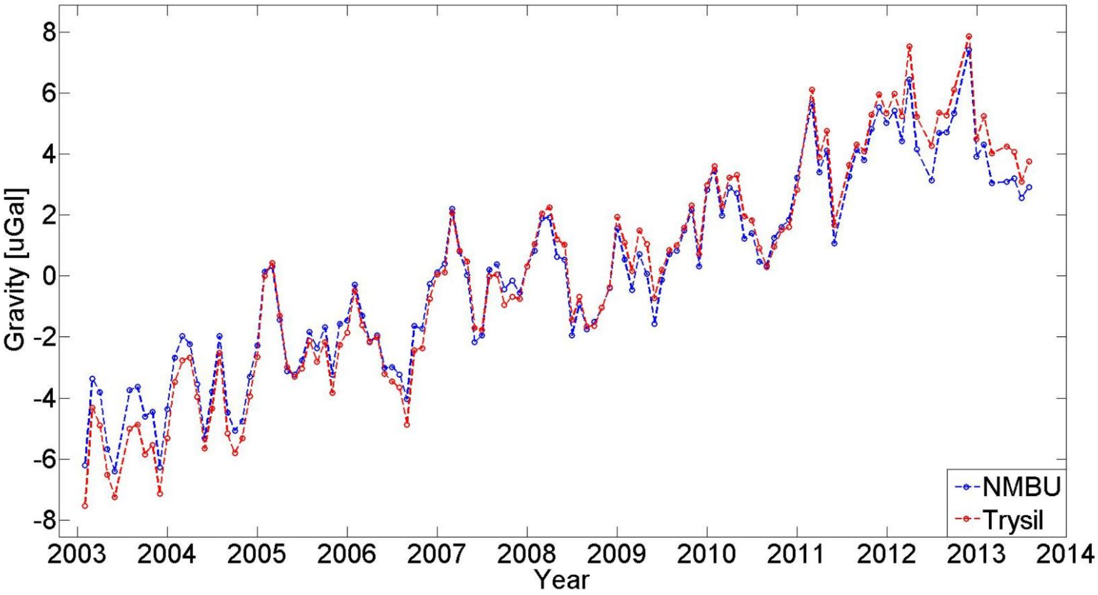

Figure 6.1: Comparison of gravity signal for NMBU and Trysil, computed from GRACE observations.

As shown in figure 6.1, the gravity signal for NMBU and Trysil is very similar. This is due to the distance of 200 kilometres between the two station. However, the absolute gravity values differ due to difference in geocentric distance.

6.2.1 NMBU, Ås

In section 4.3.1, the estimated rate of change in annual gravity was -1.3 microgals per year at NMBU. This value exceeded the rate of change value from the GIA model (equation 4.3), which was -0.8 microgals per year. As already stated, GRACE is orbiting the Earth at an altitude of 500 kilometres and cannot detect change in gravity due to GIA induced vertical displacement. GRACE can only detect GIA in form of mass displacement. From equation 4.1 to 4.3, the GRACE observed change in gravity should be at the same rate as observed by the FG5. However, the change in gravity will be observed as a positive trend.

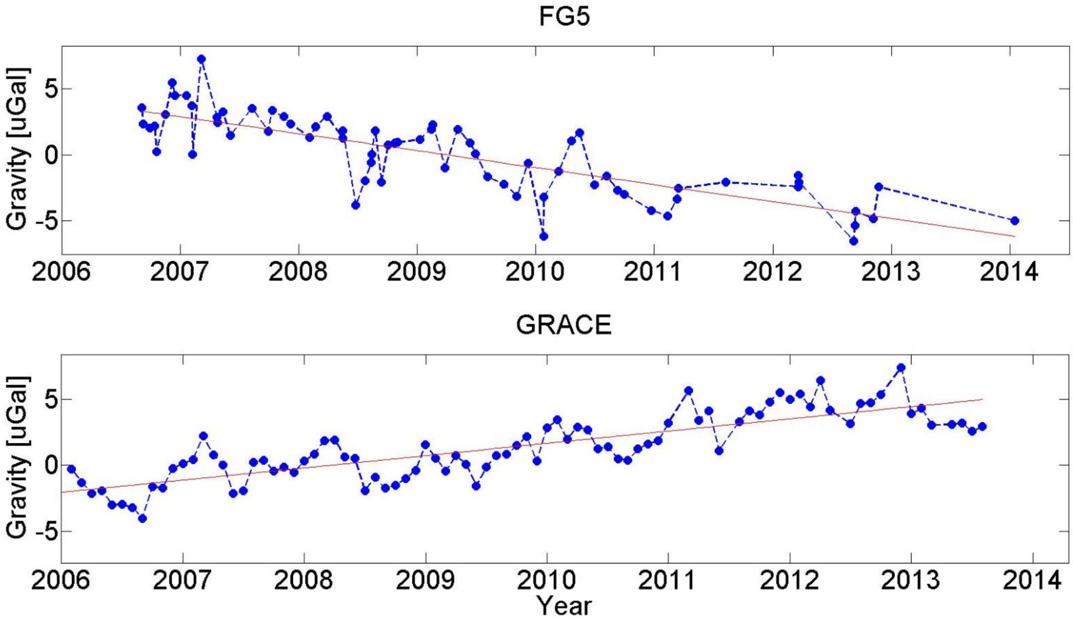

Figure 6.2: Comparison of FG5 data and GRACE from 2006 to 2014 at NMBU.

In figure 6.2 the GRACE observations estimate the rate of change in gravity to be 0.9 microgals per year. This value is in the expected range, considering the FG5 observations. As earlier mentioned, GRACE has a footprint of 300 kilometres. This means that the local gravity value at NMBU is an averaged value over such an area. For that reason, some deviations should be expected when comparing GRACE observations to terrestrial observations.

In figure 6.3, a comparison of seasonal gravity variations from FG5 and GRACE data is shown. As shown, the two sets of observations are correlated. However, there are some deviations, which can be explained by the footprint versus point value quandary. Also, GRACE observes a smoothed gravitational signal because the gravitational force is inversely proportional to the geocentric distance, cf. Newton's law of universal gravitation.

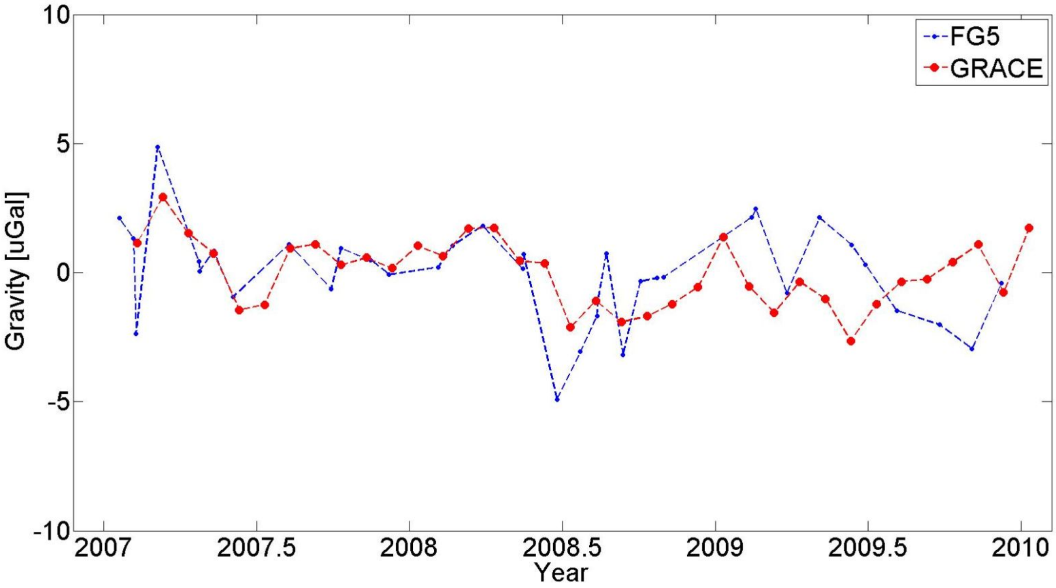

Figure 6.3: Comparison of FG5 data and GRACE from 2007 to 2010 at NMBU. Both datasets have been corrected for GIA.

6.2.2 Trysil

In section 4.3.2, the rate of change in annual gravity was estimated to be -1.2 microgals per year for Trysil. This estimate agreed completely with the theoretical GIA model. On the basis of GRACE observations, the annual rate of change in gravity is 1.3 microgals per year (see figure 6.4). This agrees quite well with the FG5 results.

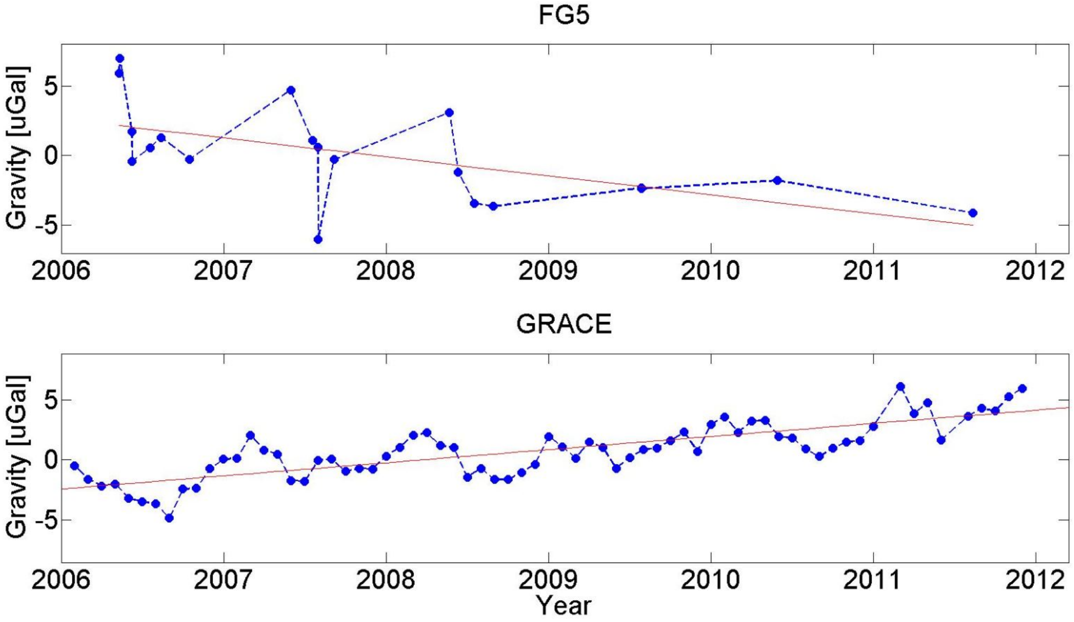

Figure 6.4: Comparison of FG5 data and GRACE from 2006 to 2012 in Trysil.

A comparison of semi-annual gravity variations based on FG5 data and GRACE data is shown in figure 6.5. As for the NMBU station, there is a correlation between the two datasets. The figure also indicates that GRACE cannot capture the full extent of seasonal variations in Trysil, as GRACE observations are based on an averaged gravity value.

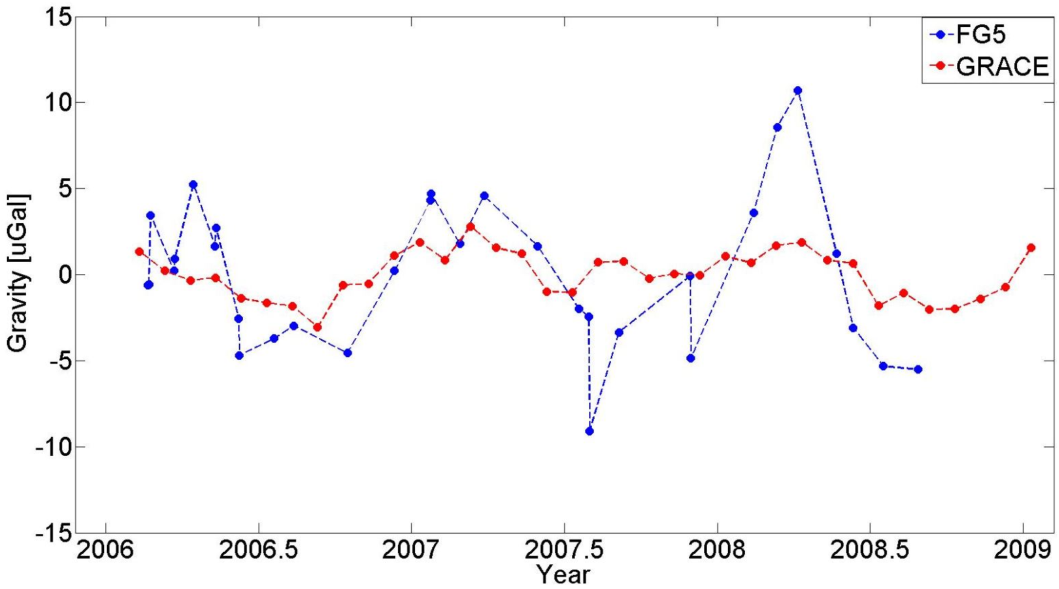

Figure 6.5: Comparison of FG5 data and GRACE from 2006 to 2009 in Trysil. Both datasets have been corrected for GIA.

Even though load induced snow cover effects have been estimated by implementing the load love numbers, there is a significant deviation in the two datasets shown in figure 6.5. The regional snow loading effects in southern parts of Norway correspond to approximately 1 microgal (Breili and Pettersen, 2009). 90 percent of the snow induced gravity variations in Trysil is generated by the snow cover within 200 meters from the laboratory, as shown by Breili and Pettersen (2009). GRACE cannot detect these local effects, which causes the deviation between the two datasets.

6.2.3 Ny-Ålesund

In section 4.4.3, the rate of change in annual gravity was estimated to be -1.6 microgals per year. The theoretical estimate using the GIA model was equal to -1.3 microgals per year. Like previously discussed, the land uplift in Ny-Ålesund is a bit more complex. The total land uplift is over 8 millimetres. However, the GIA induced land uplift is only 2 millimetres (Kierulf, 2012). If only the GIA induced land uplift is considered, the expected rate of change in gravity would be -0.3 microgals per year (cf. equation 4.3).

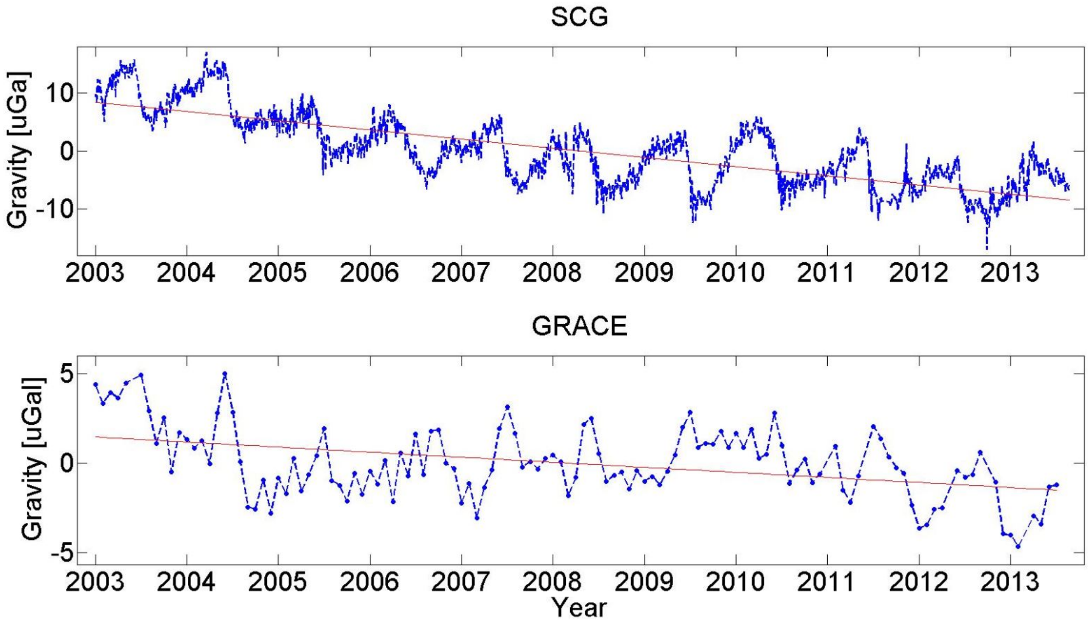

Figure 6.6: Comparison of SCG data and GRACE from 2003 to 2011 in Ny-Ålesund.

The GRACE observations estimate the rate of change in gravity to be -0.3 microgals per year. This might indicate that the GIA signal cannot be found in GRACE observations covering Ny-Ålesund. GRACE observe GIA as mass displacement due to compressed land when Svalbard was covered with ice during the last glacial period. The local land uplift is due to loss of mass in form of ice melting today. This is something GRACE will observe as a decrease in mass. Hence, an increase in gravity corresponding to the decrease in gravity estimated by the superconducting gravimeter should not be expected.

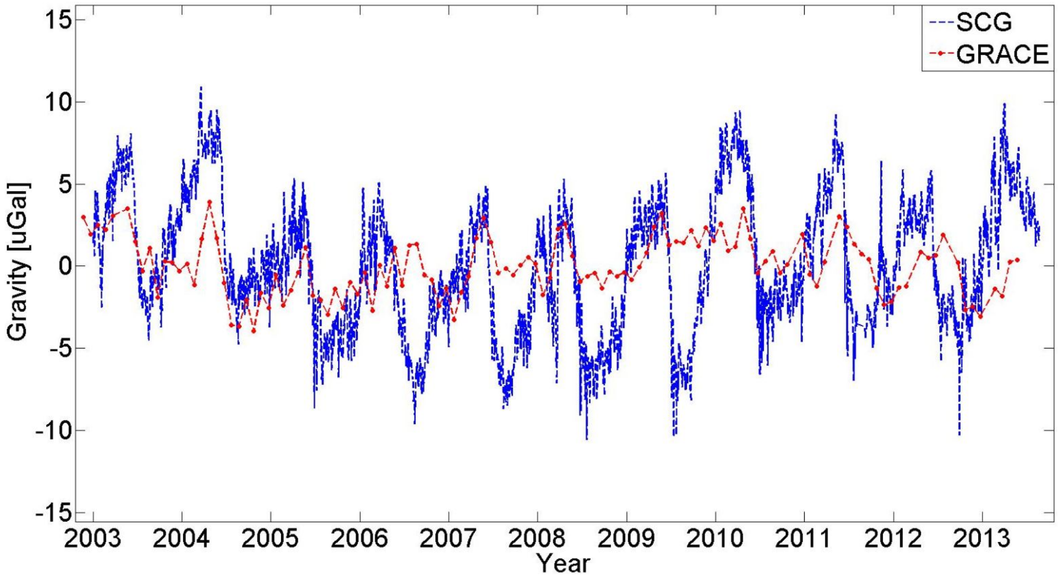

Figure 6.7: Comparison of SCG data and GRACE from 2003 to 2013 in Ny-Ålesund. Both datasets have been corrected for GIA.

The final comparison is given between the superconducting gravimeter and GRACE in Ny-Ålesund (see figure 6.7). Although there is correlation between the two datasets, it is possible observe that GRACE does not fully account for all seasonal variations in Ny-Ålesund.

Table 6.1: GIA analysis

Station	Period	GIA model	FG5/SCG	GRACE
NMBU	2006 - 2014	-0.8 $\frac{\mu Gal}{yr}$	-1.3 $\frac{\mu Gal}{yr}$	0.9 $\frac{\mu Gal}{yr}$
Trysil	2006 - 2011	-1.2 $\frac{\mu Gal}{yr}$	-1.2 $\frac{\mu Gal}{yr}$	1.1 $\frac{\mu Gal}{yr}$
Ny-Ålesund	2003 - 2011	-1.3 $\frac{\mu Gal}{yr}$	-1.6 $\frac{\mu Gal}{yr}$	-0.3 $\frac{\mu Gal}{yr}$

Chapter 7

Conclusions and further outlook

Earth's gravity field is a complexed physical matter, and cannot be fully expressed and understood using Newton's law of universal gravitation. By introducing potential theory, interpretations can be started in order to analyse some of the many constituents that make up Earth's attraction on other objects.

Spherical harmonic synthesis is one outcome of potential theory. It can be used to derive potential differences between the mathematical Earth model, known as the ellipsoid, and the physical shape of the Earth, known as the geoid. This can again lead to estimation of geophysical signals found in Earth's gravity field.

This chapter tries to summaries the previous chapters, and provide some final conclusions.

7.1 Terrestrial gravimetry

Terrestrial gravimetry can be categorized into two different techniques. One is relative gravimetry, where relative gravity variations are measure. The other is absolute gravimetry, where absolute gravity is measured. Because there are two different methods, and both methods are highly accurate, terrestrial gravimetry has a wide variety of applications. In chapter 4, investigations have been carried out to see how terrestrial gravity observations can be used to derive geophysical signals in Earth's gravity field. Observations gathered at three different stations have been used in order to derive local gravity variations. It has been shown that solid Earth tides and ocean loading has a combined impact on gravity by the amount of ± 50 microgals in Trysil. This has to be corrected if studies of other geophysical phenomena should be carried out.

At NMBU the observed rate of change in gravity due to GIA was -1.3 microgals per year. If this estimate is used to calculate annual land uplift, the result is 8.7 millimetres per year. This estimate is higher when compared to other estimates from this region. Observations also indicated that the seasonal gravity variations at NMBU are very small, which means that local hydrological variations are not very significant.

In Trysil the estimate rate of change in gravity was -1.2 microgals per year. If the estimate is used to calculate GIA induced land uplift, the result is 8.0 millimetres per year. Seasonal variations are present to a far greater extent in Trysil, when compared to NMBU. In section 4.3.2, it is shown that gravity variations are highly correlated with snow water equivalent variations. This means that hydrological variations are the main causes of seasonal graivty variations in Trysil.

In section 4.3.3, the estimated rate of change in gravity in Ny-Ålesund was -1.6 microgals per year, which correspond to a land uplift rate of 10.7 millimetres per year. The superconducting gravimeter observations indicate that there is a variation in the annual rate of land uplift. This is caused by local land uplift, due to the ongoing ice melting Ny-Ålesund experience today. Like Trysil, the Ny-Ålesund station see seasonal gravity variations to a far greater extent, when compared to NMBU.

Terrestrial observations are vital for accurate determination of Earth's gravity field, as it is independent from external reference frames (Breili, 2011). It is, and will continue to be, used to study GIA, hydrological variations, changes in the Earth's cryosphere and other geophysical phenomena. It also plays a substantial part in realization of gravity networks and height datums. In addition, terrestrial gravimetry is important when it comes to satellite gravimetry as well. Terrestrial observations are in many cases used to validate satellite based observations.

Terrestrial gravimetry instruments are sensitive to mechanical and electronic errors. New and improved instruments are being developed, both to improve the accuracy, and to make the instruments more sustainable.

7.2 Satellite gravimetry

Observing Earth's gravity field from space has been carried out for decades. It started of with SLR based observations in the late 1960s. Through the dedicated gravity satellite missions CHAMP (2000), GRACE (2002) and GOCE (2009), global potential models have given us a better understanding of Earth's gravity field on a global scale.

In chapter 5, examinations of how GRACE can be used to detect seasonal variations in Earth's gravity field have been carried out. Seasonal variations on a global scale (section 5.4.2) show hydrology variations in the Amazon and southern parts of Africa. In section 5.4.1, global gravity field variations covering several years is displayed. These observations indicate a GIA induced land uplift in the northern parts of North-America, Antarctica and Fennoscandia. There is also a significant decrease in mass found in Greenland, West-Antarctica and Alaska, due to ice melting.

When comparing satellite data and terrestrial data, there are some methodology differences that have to be taken into account, like gravity versus gravitation and footprint observation versus point observation. In an analysis covering several years, GRACE observe GIA as a positive trend due to mass displacement. The FG5 observations, however, observe a corresponding negative trend, due to vertical displacement. This difference is shown in the comparison made for NMBU and Trysil.

When estimating seasonal gravity variations, observations show that GRACE does not account for the full extent of these seasonal variations. This is because GRACE provides an averaged point value over an area of 300 kilometres. In parts of the world that experience severe gravity variations locally, GRACE cannot be used to analyse these variations.

In the years 2011 and 2012, there were observed noise in the GRACE monthly solutions. There were also some observational gaps in this period. This might indicate that some operational errors took place at that time. However, the noise disappeared when C_{20} was replaced by SLR observations.

There is a GRACE follow-on mission approaching, indicating dedicated gravity satellite missions are an area of interest also in the future. Studies have shown the wide variety of applications of such satellites, including geophysical research.

Bibliography

Barthelmes, F. (2009). *Definition of functionals of the geopotential and their calculation from spherical harmonic models.* Deutsches Geo-ForschungsZentrum GFZ.

Biancale, R., Balmino, G., Lemoine, J.-M., Marty, J.-C., Moynot, B., Barlier, F., Exertier, P., Laurain, O., Gegout, P., Schwintzer, P., et al. (2000). A new global earth's gravity field model from satellite orbit perturbations: Grim5-s1. *Geophysical Research Letters*, 27(22):3611–3614.

BKG (2010). Satellite laser ranging. `http://www.iers.org/nn_11666/IERS/EN/Science/Techniques/slr.html?__nnn=true`. Accessed: 2014-02-27.

Boy, J.-P. and Hinderer, J. (2006). Study of the seasonal gravity signal in superconducting gravimeter data. *Journal of Geodynamics*, 41(1):227–233.

Breili, K. (2011). The role of absolute gravity measurements in the 21 century. *Kart og Plan*, 71:133–144.

Breili, K. and Pettersen, B. R. (2009). Effects of surface snow cover on gravimetric observations. *Journal of Geodynamics*, 48(1):16–22.

Case, K., Kruizinga, G., and Wu, S. (2002). Grace level 1b data product user handbook. *JPL Publication D-22027*.

Chambers, D. P. (2006). Observing seasonal steric sea level variations with grace and satellite altimetry. *Journal of Geophysical Research: Oceans (1978–2012)*, 111(C3).

Gerlach, C. (2003). *Zur Höhensystemumstellung und Geoidberechnung in Payern.* Deutsche Geodäische Kommision. Ph.D. thesis.

GFZ (2013). Glacial isostatic adjustment. `http://www.gfz-potsdam.de/en/research/organizational-units/departments/department-1/earth-system-modelling/topics/ice-sheet-and-solid-earth-dynamics/glacial-isostatic-adjustment-gia/`. Accessed: 2014-04-01.

Helmert, F. R. (1880). *Die mathematischen und physikalischen theorieen der höheren geodäsie*. BG Teubner.

Hofmann, F., Müller, J., and Biskupek, L. (2010). Lunar laser ranging test of the nordtvedt parameter and a possible variation in the gravitational constant. *A&A*, 522:L5.

Hofmann-Wellenhof, B. and Moritz, H. (2006). *Physical geodesy*. Springer.

Kartverket (2012). Landhevning i norge. `http://www.kartverket.no/Kunnskap/Klimaforskning/Landheving-i-Norge/`. Accessed: 2014-04-18.

Kierulf, H. P. (2012). Havnivå og landheving på svalbard. `http://sehavniva.no/tema/landheving/havniva-og-landheving-pa-svalbard/`. Accessed: 2014-04-22.

König, R., Chen, Z., Reigber, C., and Schwintzer, P. (1999). Improvement in global gravity field recovery using gfz-1 satellite laser tracking data. *Journal of Geodesy*, 73:398–406.

Kusche, J., Schmidt, R., Petrovic, S., and Rietbroek, R. (2009). Decorrelated grace time-variable gravity solutions by gfz, and their validation using a hydrological model. *Journal of Geodesy*, 83(10):903–913.

Lysaker, D. I. (2011). Recent satellite gravity missions and their applications in the geosciences. *Kart og plan*, 71:266–273.

Marengo, J. A., Liebmann, B., Kousky, V. E., Filizola, N. P., and Wainer, I. C. (2001). Onset and end of the rainy season in the brazilian amazon basin. *Journal of Climate*, 14(5):833–852.

Milyukov, V. and Fan, S.-h. (2012). The newtonian gravitational constant: Modern status of measurement and the new codata value. *Gravitation and Cosmology*, 18(3):216–224.

NASA (2012). Grace - mission overview. `http://www.nasa.gov/mission_pages/Grace/overview/index.html`. Accessed: 2014-03-06.

Neumeyer, J. (2010). Superconducting gravimetry. In *Xu (ed.) Sciences of Geodesy-I*, pages 339–406. Springer.

Neumeyer, J., Barthelmes, F., Kroner, C., Petrovic, S., Schmidt, R., Virtanen, H., and Wilmes, H. (2008). Analysis of gravity field variations derived from superconducting gravimeter recordings, the grace satellite and hydrological models at selected european sites. *Earth Planets and Space*, 60(5):505.

Omang, O. and Kierulf, H. (2011). Past and present-day ice mass variation on svalbard revealed by superconducting gravimeter and gps measurements. *Geophysical Research Letters*, 38(22).

Peters, T. (2001). *Zeitliche Variationen des Gravitationsfeldes der Erde.* Inst. für Astronomische und Physikalische Geodäsie. Ph.D. thesis.

Ray, R. and Luthcke, S. (2006). Tide model errors and grace gravimetry: Towards a more realistic assessment. *Geophysical Journal International*, 167(3):1055–1059.

Reigber, C., Jochmann, H., Wünsch, J., Petrovic, S., Schwintzer, P., Barthelmes, F., Neumayer, K.-H., König, R., Förste, C., Balmino, G., et al. (2005). Earth gravity field and seasonal variability from champ. In *Earth Observation with CHAMP*, pages 25–30. Springer.

Rummel, R., Balmino, G., Johannessen, J., Visser, P., and Woodworth, P. (2002). Dedicated gravity field missions principles and aims. *Journal of Geodynamics*, 33(1):3–20.

Sanz Subirana, J., Juan Zornoza, J., and Hernandez-Pajares, M. (2011). Ocean loading. `http://www.navipedia.net/index.php/Ocean_loading`. Accessed: 2014-04-01.

Seeber, G. (2003). *Satellite Geodesy.* Walter de Gruyter.

Sheard, B., Heinzel, G., Danzmann, K., Shaddock, D., Klipstein, W., and Folkner, W. (2012). Intersatellite laser ranging instrument for the grace follow-on mission. *Journal of Geodesy*, 86(12):1083–1095.

Shiomi, S. (2009). Testing gravitational physics with superconducting gravimeters. *arXiv preprint arXiv:0902.4081.*

Timmen, L. (2010). Absolute and relative gravimetry. In *Xu (ed.) Sciences of Geodesy-I*, pages 1–43. Springer.

Torge, W. and Müller, J. (2012). *Geodesy.* Walter de Gruyter.

Trenberth, K. E., Christy, J. R., and Olson, J. G. (1987). Global atmospheric mass, surface pressure, and water vapor variations. *Journal of Geophysical Research: Atmospheres (1984–2012)*, 92(D12):14815–14826.

Virtanen, H. (2006). *Studies of Earth dynamics with the superconducting gravimeter.* University of Helsinki. Ph.D. thesis.

Vonbun, F., Weightman, J., Wilson, P., and Elsmore, B. (1977). Goddard laser systems and their accuracies [and discussion]. *Philosophical Transactions of the Royal Society of London. Series A*, 284:443–450.

Wahr, J., DaZhong, H., and Trupin, A. (1995). Predictions of vertical uplift caused by changing polar ice volumes on a viscoelastic earth. *Geophysical Research Letters*, 22(8):977–980.

Wahr, J., Molenaar, M., and Bryan, F. (1998). Time variability of the earth's gravity field: Hydrological and oceanic effects and their possible detection using grace. *Journal of Geophysical Research: Solid Earth (1978–2012)*, 103(B12):30205–30229.

Wouters, B. (2010). *Identification and Modeling of Sea Level Change Contributors: On GRACE satellite gravity data and their applications to climate monitoring.* Delft University of Technology. Ph.D. thesis.

Appendices

Appendix A

Global approach 2007 - 2009

This appendix contain the geoid variation maps from 2007 to 2009 interpreted in section 5.4.3, subsection "Global approach". The maps are based on a seasonal analysis.

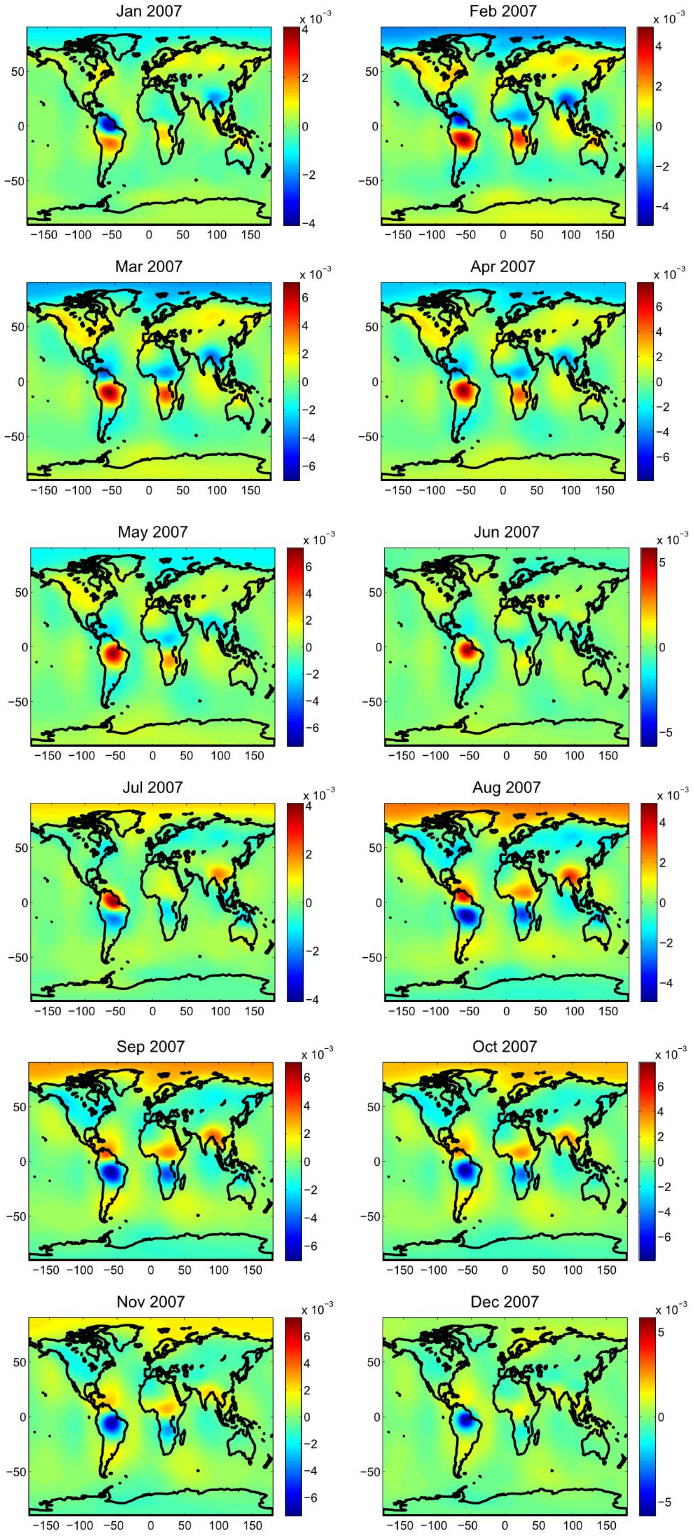

Figure A.1: Seasonal gravity field variations in terms of geoid height variation [m]. January - December, 2007.

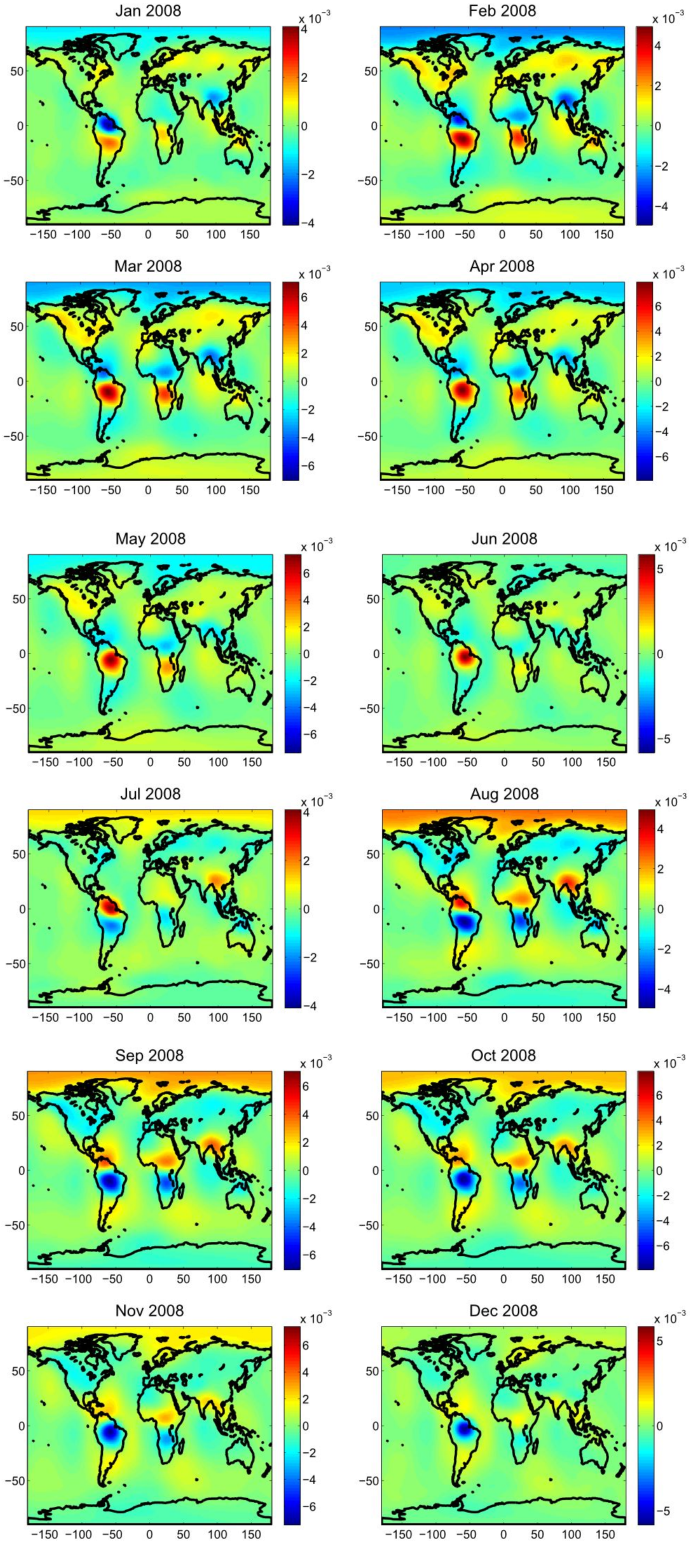

Figure A.2: Seasonal gravity field variations in terms of geoid height variation [m]. January - December, 2008.

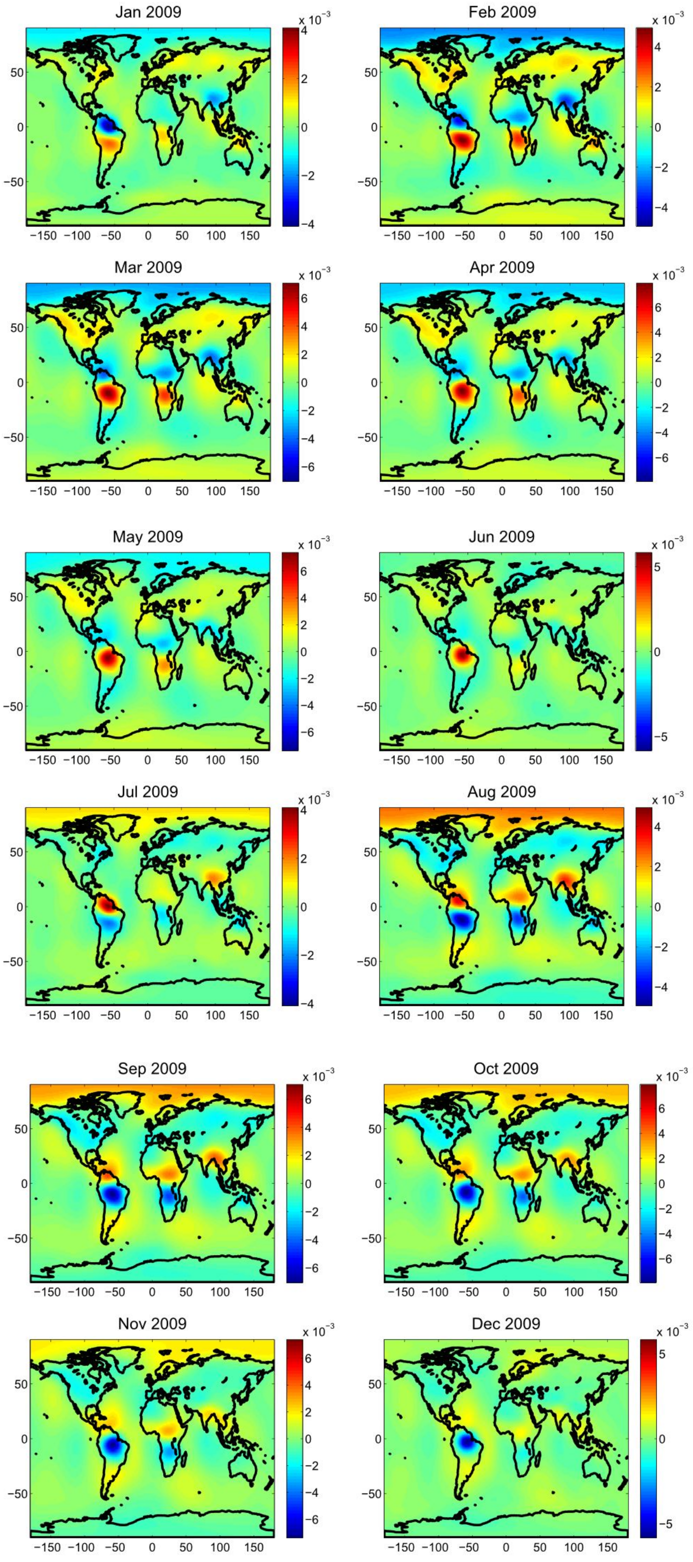

Figure A.3: Seasonal gravity field variations in terms of geoid height variation [m]. January - December, 2009.

Norwegian University
of Life Sciences

Postboks 5003
NO-1432 Ås, Norway
+47 67 23 00 00
www.nmbu.no